Differential functional brain network connectivity during visceral interoception as revealed by independent component analysis of fMRI time-series

Jarrahi, Behnaz ; Mantini, Dante ; Balsters, Joshua Henk ; Michels, Lars ; Kessler, Thomas M ; Mehnert, Ulrich ; Kollias, Spyros S

Abstract: Influential theories of brain-viscera interactions propose a central role for interoception in basic motivational and affective feeling states. Recent neuroimaging studies have underlined the insula, anterior cingulate, and ventral prefrontal cortices as the neural correlates of interoception. However, the relationships between these distributed brain regions remain unclear. In this study, we used spatial independent component analysis (ICA) and functional network connectivity (FNC) approaches to investigate time course correlations across the brain regions during visceral interoception. Functional magnetic resonance imaging (fMRI) was performed in thirteen healthy females who underwent viscerosensory stimulation of bladder as a representative internal organ at different prefill levels, i.e., no prefill, low prefill (100 ml saline), and high prefill (individually adapted to the sensations of persistent strong desire to void), and with different infusion temperatures, i.e., body warm (37°C) or ice cold (4-8°C) saline solution. During Increased distention pressure on the viscera, the insula, striatum, anterior cingulate, ventromedial prefrontal cortex, amygdalo-hippocampus, thalamus, brainstem, and cerebellar components showed increased activation. A second group of components encompassing the insula and anterior cingulate, dorsolateral prefrontal and posterior parietal cortices and temporal-parietal junction showed increased activity with innocuous temperature stimulation of bladder mucosa. Significant differences in the FNC were found between the insula and amygdalo-hippocampus, the insula and ventromedial prefrontal cortex, and the ventromedial prefrontal cortex and temporal-parietal junction as the distention pressure on the viscera increased. These results provide new insight into the supraspinal processing of visceral interoception originating from an internal organ. Hum Brain Mapp, 2015. © 2015 Wiley Periodicals, Inc.

DOI: https://doi.org/10.1002/hbm.22929

DIFFERENTIAL FUNCTIONAL BRAIN NETWORK CONNECTIVITY DURING VISCERAL INTEROCEPTION AS REVEALED BY INDEPENDENT COMPONENT ANALYSIS OF FMRI TIME-SERIES

Behnaz Jarrahi[1, 2, 3, 4, 5], Dante Mantini[5, 6, 7], Joshua Henk Balsters[7], Lars Michels[1, 8], Thomas M. Kessler[3], Ulrich Mehnert[3], and Spyros Kollias[1, 5]

1 Clinic for Neuroradiology, University Hospital, Zurich, Switzerland

2 Department of Information Technology and Electrical Engineering, Institute for Biomedical Engineering, Federal Institute of Technology (ETH), Zurich, Switzerland

3 Neuro-Urology, Spinal Cord Injury Center, University of Zurich, Balgrist University Hospital, Zurich, Switzerland

4 Department of Psychiatry and Biobehavioral Sciences, Semel Institute for Neuroscience and Human Behavior, University of California, Los Angeles (UCLA), California

5 Neuroscience Center Zurich, University and ETH, Zurich, Switzerland

6 Department of Experimental Psychology, University of Oxford, Oxford, United Kingdom

7 Department of Health Sciences and Technology, Neural Control of Movement Laboratory, ETH Zurich, Switzerland

8 Center for MR-Research, University Children's Hospital, Zurich, Switzerland

Hum Brain Mapp. 2015 Nov;36(11):4438-68

PMID: 26249369

DOI: 10.1002/hbm.22929

ABSTRACT

Influential theories of brain-viscera interactions propose a central role for interoception in basic motivational and affective feeling states. Recent neuroimaging studies have underlined the insula, anterior cingulate, and ventral prefrontal cortices as the neural correlates of interoception. However, the relationships between these distributed brain regions remain unclear. In this study, we used spatial independent component analysis (ICA) and functional network connectivity (FNC) approaches to investigate time course correlations across the brain regions during visceral interoception. Functional magnetic resonance imaging (fMRI) was performed in thirteen healthy females who underwent viscerosensory stimulation of bladder as a representative internal organ at different prefill levels, i.e., no prefill, low prefill (100 ml saline), and high prefill (individually adapted to the sensations of persistent strong desire to void), and with different infusion temperatures, i.e., body warm (~37°C) or ice cold (4–88°C) saline solution. During Increased distention pressure on the viscera, the insula, striatum, anterior cingulate, ventromedial prefrontal cortex, amygdalo-hippocampus, thalamus, brainstem, and cerebellar components showed increased activation. A second group of components encompassing the insula and anterior cingulate, dorsolateral prefrontal and posterior parietal cortices and temporal-parietal junction showed increased activity with innocuous temperature stimulation of bladder mucosa. Significant differences in the FNC were found between the insula and amygdalo-hippocampus, the insula and ventromedial prefrontal cortex, and the ventromedial prefrontal cortex and temporal-parietal junction as the distention pressure on the viscera increased. These results provide new insight into the supraspinal processing of visceral interoception originating from an internal organ.

Keywords: fMRI; insula; prefrontal; salience; self-referential; limbic; homeostasis; bladder; visceral sensation; alliesthesia

INTRODUCTION

Interoception collectively refers to the sensing, representation and perception of the physiological condition of the body arising from the afferent information anywhere and everywhere within the body [1, 2]. Interoception is closely associated with the endogenous homeostatic mechanisms necessary for survival and prosperity, and underlies affective states and fundamental cognitive processes in human [3-6]. It can be contrasted with the exteroceptive systems that keep the individual organism aware of the external environment as opposed to the bodily or self-referential (introspectively-oriented) processes [2]. However, in contrast to the rich history of studying the exteroceptive senses and their well-recognized sensory cortical systems, less is known about the neural substrates that provide the brain with a dynamic representation of the body.

Neuroanatomical evidence suggests that information concerning the internal state of the body—including mechanical, thermal, chemical, osmotic, and hormonal aspects—is not only relayed to the spinal cord for autonomic reflexes, but the information is also projected to supraspinal regions [2, 4, 7]. In particular, the Aδ- and C-fiber projection to a specific lamina I spinothalamocortical pathway as well as the vagal and glossopharyngeal afferents to the parabrachial nucleus in brainstem via the nucleus of the solitary tract in medulla, have been proposed to carry sympathetic and parasympathetic afferents related to homeostatic and autonomic activities to the brain [2, 4]. For example, in the case of a visceral organ such as the urinary bladder (UB), the Aδ-fibers are mechanosensors (more specifically tension receptors) responsible for the physiologic sensation of fullness [8, 9]. The C-fibers are generally insensitive to intravesical pressure but given their proximity to the intravascular milieu [10], they respond to cooling [11] or chemical irritation of the mucosa [12]. Modality-specific lamina I neurons primarily project to autonomic cell columns in the spinal cord, where sympathetic preganglionic motoneurons are located, and to the integration homeostatic sites in the brainstem [13]. In primates, lamina I neurons also project topographically to two relay nuclei in thalamus: the posterior part of the ventral medial nucleus [14, 15], and the ventral caudal part of the medial dorsal nucleus [13]. The posterior part of the ventral medial nucleus is contiguous rostrally with the basal part of the ventral medial thalamic nucleus, which receives a direct input from the nucleus of the solitary tract (i.e. parasympathetic afferent input) in addition to the lamina I inputs (i.e. sympathetic afferent input). The posterior part of the ventral medial nucleus eventually projects to the interoceptive cortex in the posterior insula [16]. The ventral caudal part of the medial dorsal nucleus, which receives projection from the parabrachial nucleus in the brainstem in addition to the lamina I inputs, projects to the anterior cingulate cortex (ACC) [13]. According to the "homeostatic emotion" proposition of interoception [2, 13, 17], in humans the integration of afferent physiological signals with higher order contextual information, motivational state, and previously learned associations, is postulated to occur upon further propagation of interoceptive (homeostatic sensory) inputs from the interoceptive cortex in the posterior insula to the anterior insula [18], the ACC, and the ventral prefrontal cortices (PFC) [17, 19, 20]. In line with this proposition, neuroimaging studies of interoception including those involving somesthesis (e.g. nociception; [21]), autonomic arousal [22-24], viscerosensory stimulation [25-27], somatic control (including the regulation of cardio-regulatory, vasomotor and visceromotor activity; e.g., [28]), temperature [29], dyspnea [30], thirst [31, 32], hypoglycemia [33], satiety and craving [34]

have substantiated activation in the insula, the ACC, and the PFC among other paradigm-specific cortical and subcortical regions when bodily states significantly deviated from the steady state.

Few studies have used multivariate approaches such as the independent component analysis (ICA) [35-37] and multi-voxel pattern analysis [38] to investigate brain activation during interoception. For example, using a pattern recognition analytical technique, Björnsdotter et al. [199] reported an anteroposterior somatotopic organization in dorsal posterior insula caused by gentle touch (i.e., slow brush stimulation of C-fiber tactile afferents). Liu et al. [200] applied support vector machine technique, a multivariate pattern analysis method, to investigate the differences of resting-state function mapped by regional homogeneity in patients with functional dyspepsia. The results showed highly discriminative brain regions mainly included the PFC involving the orbitofrontal cortex, supplementary motor area, insula, anterior/middle cingulate, thalamus, hippocampus/ parahippocampus, and cerebellum. Hojo et al. [77] used ICA approach to analyze brain activity during intraesophageal infusion of acid and saline in six healthy males and observed the common cerebral regions activated with saline and HCl infusion were the thalamus, insula, cingulate, and portions of the frontal, temporal, and parietal cortices. Similarly, Hall et al. [76] applied ICA as a multivariate analysis technique to assess brain networks during a single slow ramp-tonic rectal distension in seven females with irritable bowel syndrome and six healthy females and demonstrated that patients with irritable bowel syndrome had increased activation of the insula, ACC and ventromedial PFC while healthy controls showed increased activation in the thalamus, striatum and dorsolateral PFC.

Despite recent advances in understanding the neural correlates of interoception, still it is not clear how these distributed neural systems in the brain are functionally connected during the interoceptive processing. The study of functional connectivity is concerned with the temporal coherence among spatially remote brain regions [39]. In the traditional functional connectivity analysis, time courses of individually selected seed voxels from predefined brain regions of interest are cross correlated with other voxels' time courses to identify voxels showing significant connectivity with the seed voxels [40, 41]. An alternative approach is the ICA-based functional network connectivity (FNC), which is a data-driven method that measures the statistical dependencies among maximally spatially independent configurations of voxel weightings (referred to as independent components) [42, 43]. Networks [44] obtained in this way are characterized by a single time course (called the mixing coefficients) [42], and have been shown to track closely with previously identified functional domains [45, 46].

Studying task-induced modulations and dynamics of brain networks during interoception can provide more details on how brain process afferent visceral signals originating within the body. Furthermore, understanding the neural regulation of visceral function and sensation provides essential insights into the biological basis of emotion and feeling [5, 17, 47-50]. The main aim of this study, therefore, was to extend previous research by

1. Exploring the modulation of brain networks identified with ICA during the viscerosensory stimulation.
2. Examining the time course correlations across these networks (FNC) during different visceral interoceptive conditions.

To study network modulation and dynamics during interoception, spatiotemporal control of the viscerosensory stimulation is necessary. The UB was selected as a designated visceral organ to deliver direct viscerosensory stimulations since it differs from other visceral organs in its pattern of activity and in the organization of its neural control mechanisms [51]. Specifically, the neural circuits that control the UB function (i.e., urine storage and elimination) have phasic (switch-like) patterns of activity, which contrasts the tonic patterns of the autonomic pathways that regulate the cardiovascular organs. Furthermore, micturition is a learned behavior hence under voluntary control whereas many other visceral functions such as digestion are regulated involuntarily [51]. Previous functional brain imaging studies of continence have identified several cortical and subcortical regions involved in the normal sensation of the UB fullness. These areas include the insula, predominately on the right [52-62], the ACC [52-54, 57-59, 61-66], right inferior frontal gyrus (IFG) [52, 54, 58, 63], PFC including orbitofrontal cortex [58], thalamus [53, 55-57, 59, 66], right middle temporal gyrus [58, 61], inferior parietal cortex [58], basal ganglia [57, 60, 66, 67], midbrain periaqueductal gray (PAG) [52, 53, 55-57, 59, 63, 64, 66], brainstem pons [52, 53, 59, 63, 64, 66] and the cerebellum [53-55, 58, 66-68]. Additionally, neuroimaging of innocuous temperature stimulation of the UB mucosa by the intravesical ice water instillation showed enhanced activations in the frontal and parietal lobes including the bilateral inferior parietal lobe, right insula, right middle temporal gyrus and the right cerebellum [69].

The pattern of regional brain activations during the distention pressure on the viscera due to the UB fullness shows similarity to the matrix of brain regions implicated in control of the gastrointestinal (GI) tract [27, 70], which indicates some overlap in neural regulations of visceral function. A systematic review of neuroimaging data of GI visceral stimulation identified key regions of activation to include the insula (both anterior and posterior sections) and the ACC, followed (in order of reported frequency) by primary sensory cortex, PFC especially the orbitofrontal cortex, posterior parietal cortex, and thalamus [71, 72]. Furthermore, psychological factors including the cognitive influences such as learning, anticipation, attention/ distraction, and emotional features like positive or negative affect, unpleasantness, and emotional context or state have shown to modulate the brain processing of visceral sensation in the ACC, insula, and sensory cortices [73-75]. However, compared to the GI viscerosensory stimulations studies, only few neuroimaging studies of the UB have attempted to identify the connectivity of brain regions with some indications of their functions and interactions among the viscerosensory, affective and cognitive components of the continence/micturition circuits. Tadic et al. [61] examined the connectivity of continence-related brain regions in women with urge incontinence using physio-physiological interaction method. The results showed that in normal subjects frontotemporal and sensorimotor cortex, forebrain, midbrain and pontine region were effectively connected with the right insula and ACC (two seeds regions chosen a priori) but in the urge-incontinent subjects, the effective connectivity was shifted to a parietotemporal complex. Kuhtz-Buschbeck et al. [56] used similar approach to explore the effective connectivity of cortical regions during attempted micturition and found that mid-cingulate cortex had stronger connectivity with the PAG and medial motor regions during attempted micturition compared to the baseline while both the left and right insula showed decreased connectivity. In a more recent study, Michels et al. [59] performed seed-based correlation analysis of activated brain areas during the switch from storage to micturition and demonstrated that initiation of micturition induced major activity in the PAG, pons,

insula, thalamus, PFC, parietal operculum and cingulate cortex with significant functional connectivity between the forebrain and parietal operculum. Still further research is required to understand the supraspinal networks related to the sensory-perception of the visceral functions to delineate how brain perceives visceral sensations originating from within the body, detects deviation of physiological parameters, brings them into consciousness when a deviation exceeds a limit, and motivates behavior as well as appropriate motor output (e.g., micturition) to maintain homeostasis (e.g., continence). Based on previous multivariate analysis of visceral interoception [76, 77] as well as previous conventional (univariate) fMRI analyses of the UB viscerosensory stimulations that we had performed (i.e., [58, 59, 67, 69, 78]), our hypothesis was that visceral interoception of the UB (i.e., the mechanical distention and temperature stimulation of the mucosa) would modulate the brain networks specifically related to the stimulus-driven detection of salient stimuli including the insula and ACC. We further expected that during the gradual increase of distention pressure on the viscera (from the first sensation of filling to strong desire to void), FNC between the interoceptive cortex and subcortical structures involved in affective and motivational dimensions, such as amygdala and ventral striatum [79], as well as higher order areas related to executive control of the micturition inhibition such the medial PFC [80] would be altered.

MATERIALSAND METHODS

PARTICIPANTS

Fifteen healthy, right-handed female participants (age range 21 – 48) with no history of neurological, major medical, or psychiatric disorder participated in the study. Since there are some evidences in the literature indicating gender differences in brain response to viscerosensory stimulation [56, 81-83], only female participants were recruited. All participants underwent comprehensive clinical evaluation including (i) detailed medical history, (ii) completion of a three-day voiding diary providing information on voiding frequency and volumes, amount of fluid intake, and degree of desire to void, (iii) completion of validated German version of the questionnaires on lower urinary tract function and symptoms (used with the permission of the International Consultation on Incontinence Modular Questionnaire, Bristol Urological Institute, Southmead Hospital Bristol, UK) [84], and (iv) urodynamic measurements [85] to ensure the health of the participants. The urodynamic test included the filling cystometry and pressure flow studies of voiding involving the precise measurements of the Intravesical and abdominal pressures. UB sensations were evaluated in relation to the UB filling volume during filling cystometry and comprised assessments of the first sensation (when a participant first becomes aware of the UB filling), first desire to void (UB volume that leads a participant to pass urine at the next convenient moment, but voiding can be delayed if necessary), and strong desire to void (a persistent desire to void without the fear of leakage) [86]. [TQ1]Written, informed, IRB approved consent were collected from every participant, and monetary compensation was provided. Two of the participants did not complete one of the functional tasks, and their data were subsequently discarded. The data from the remaining thirteen participants (31.7 ± 8.4 years, mean ± SD) were analyzed further.

TASK DESIGN

The study design is derived from previous investigations of viscerosensory stimulation task that consists of controlled filling and emptying of the UB alternating with rest and subjective ratings [53, 58, 65, 69]. To deferentially stimulate this visceral organ, intravesical infusion was performed at different prefill levels, i.e., no prefill, low prefill (100 ml saline), and high prefill (individually adapted to the sensations of persistent strong desire to void [86] measured from maximum cytometric capacity during the pre-scan urodynamic test), and with different infusion temperatures, i.e., body warm (~37°C) or ice cold (4–88°C) saline solution (0.9% NaCl, B Braun Melsungen AG, Germany) (**Figure 1A–C**). The intravesical instillation of cold saline (ice water test) has been routinely used as a supplement to routine cystometry especially in conditions such as spinal cord injury or multiple sclerosis for evaluation of the cold-sensitive receptor via the afferent C-fiber [87, 88]. Although opinion varies with respect to thermal sensitivity of the UB mucosa [89-91], intravesical instillation of 4–8°C saline is considered innocuous and any pain during ice water test distinguishes clinical UB hypersensitivity [92] induced by pathological conditions including inflammation and hypertrophy [93]. To avoid potential influences of the menstrual cycle on viscerosensory sensitivity [94], or possible interference of menstrual pain with the experiment, participants were scanned during days 14–28, i.e., the luteal phase, of their menstrual cycle.

Upon entering the scanner, participants were catheterized transurethrally and a high-resolution T1 image was acquired. During a break, each participant underwent training to become familiar with a rating apparatus and the procedure of the fMRI scan. They were instructed to focus on their pain and desire to void sensations during stimulus administration, wait for the appearance of the visual analogue scale on the screen, and rate their sensations by taking the self-perspective from 0 (no desire to void/no pain) to 10 (strongest desire to void/most intense pain imaginable) using a custom-built fMRI-compatible handheld response system [95, 96]. They were asked to use their dominant right hand to rate and do it as quickly and as accurately as possible. The timing and sequencing of all stimulus events were controlled with the operational control software of an automated fMRI-compatible visceral infusion and drainage system that we developed for fMRI studies of visceral interoception to ensure precise temporal execution of visceral and visual stimuli during fMRI.

The NO-PREFILL WARM and NO-PREFILL COLD conditions each started with an empty UB. The task paradigm consisted of eight blocks of viscerosensory stimulation (15 min) with additional rest periods at the beginning (1 min) and end (1 min) of the experiment (17 min total measuring time) (**Figure 1B**). Each viscerosensory block consisted of intravesical infusion (24 s), ratings (15 s), immediately followed by an intravesical drainage lasting 60 s, and rest (jittered between 7 and 9 s). The operation of the automated infusion and drainage system was time-locked to each functional volume that was acquired via a trigger signal generated by the MRI scanner at the beginning of each volume acquisition. This allowed the precise matching of functional images with a corresponding visceral infusion and drainage epoch. Each infusion epoch consisted of a 15-s intravesical infusion of 100 ml warm (for NO-PREFILL WARM condition) or cold (for NO-PREFILL COLD condition) saline, which was performed by our fMRI-compatible device at the rate of 400 ml/min followed by a 9-s pause to ensure adequate time for the slow visceral sensation to be registered before participants rated their

sensations. During the intravesical drainage epoch, the UB was drained passively by opening the valve of a 3-way stop-cock that connected participants' catheter to a separate plastic container instead of an active drainage by the automated device to avoid possible suction of the UB mucosa at this zero prefill level.

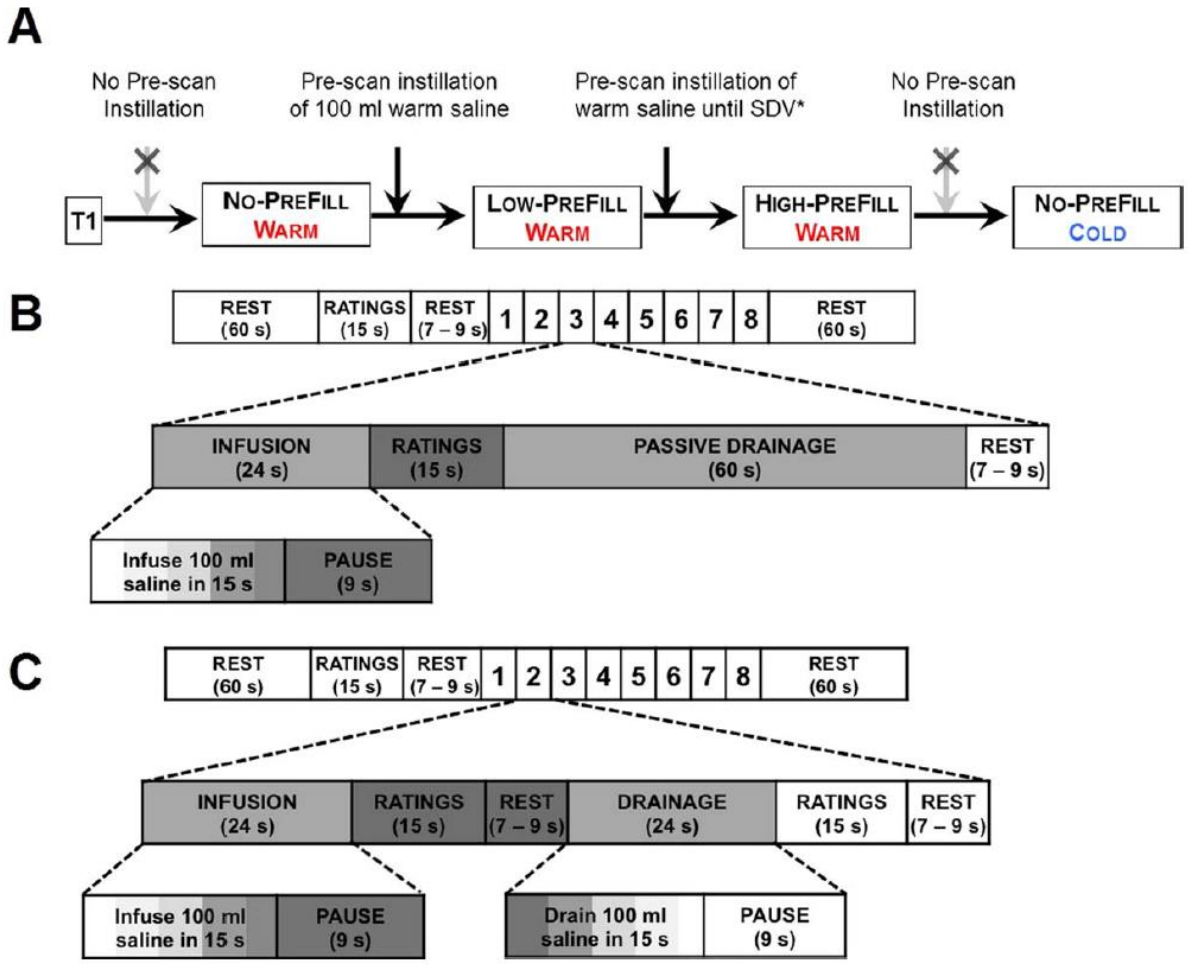

Figure 1 fMRI paradigm. (A) One anatomical (T1) and four functional conditions were performed on each participant. (B) During the NO-PREFILL conditions, eight blocks of repetitive warm or cold intravesical saline infusion, rating of sensations, and passive drainage were performed. (C) Prior to the LOW- and HIGHPREFILL conditions, pre-scan intravesical instillation of either 100 ml (for the LOW-PREFILL) or individually adapted strong desire to void (filling until strong desire to void (SDV) is achieved for HIGH-PREFILL) were completed. During the LOW- and HIGH-PREFILL conditions eight blocks of repetitive warm saline infusion and active drainage interleaved with rating of sensations were performed. *SDV: Strong desire to void.

The LOW-PREFILL WARM and HIGH-PREFILL WARM conditions started with 100 ml, and strong-desire-to-void prefilled level, respectively. Each condition consisted of eight blocks of viscerosensory stimulation (13 min) with 1- min rest periods at the beginning and end (15 min total measuring time) (**Figure 1C**). The viscerosensory block comprised an intravesical infusion (24 s), followed by ratings (15 s), and rest (jittered between 7 and 9 s), then an intravesical drainage (24 s), ratings after drainage (15 s), and rest (again jittered between 7 and 9 s). Visceral infusion and drainage were again carried out automatically by the computerized system with a 15-s intravesical infusion or withdrawal of 100 ml warm saline at the rate of 400 ml/ min and subsequent 9-s pause for a total of 24-s infusion or

drainage epoch. Since the UB cooling is an not a natural physiological event and it is considered a more intense stimuli than warm filling, and similarly the HIGHPREFILL WARM condition is a more intense stimuli than the LOW- and NO-PREFILL WARM conditions, we defined the following sequence of conditions to avoid interferences from the previous condition: all participants started with the NO-PREFILL WARM condition, followed by the LOW-PREFILL WARM condition, then the HIGHPREFILL WARM condition, and finished with the NOPREFILL COLD condition. Scanning of the participants was performed in a darkened room, with either a fixation crosshair (while subjects were not rating) or the visual analogue scale (during rating) projected via an LCD projector onto a translucent screen that stood at the foot of the gantry of the MRI scanner. The participants viewed the screen from inside the scanner through a mounted mirror attached to the head coil positioned above their eyes at a 45° angle. Participants lay in supine position on the scanner table with their legs slightly abducted and comfortably resting on custom cushions.

IMAGE ACQUISITION

All images were acquired at the MRI Center of the University Hospital of Zurich on a Philips Ingenia 3T system (Best, Netherlands) using a 15-channel receive head coil. The blood oxygenation level–dependent (BOLD)-sensitive functional images were acquired by the gradient-echo echo-planar-imaging (EPI) sequence (TR/TE = 2000/30 ms, field of view = 24 cm, image matrix = 96 × 96, flip angle = 80°, slice thickness = 3 mm, inter-slice gap = 1 mm, 34 slices in ascending order). Four dummy scans were acquired at the beginning of each functional condition to ensure the signal had achieved a steady state, and were subsequently discarded. A total of 500 volumes of the entire brain were collected for each NO-PREFILL WARM and NO-PREFILL COLD condition, and 445 volumes were obtained for each LOW-PREFILL WARM and HIGHPREFILL WARM condition. A high-resolution T1-weighted anatomical scan (3D T1-FFE, TE/TR = 3.1/6.9 ms, field of view = 22 cm, matrix = 256 × 256, slices = 180, slice thickness = 0.75 mm, no gap) was also acquired for each participant for registration with the functional data and visualization purposes. An independent neuroradiologist evaluated all T1-weighted images and no gross morphological or focal abnormalities were reported for any of the participants.

STATISTICAL ANALYSIS OF ONLINE SENSATION RATINGS

The Statistical Package for the Social Sciences (SPSS, version 21.0, SPSS, Chicago, IL) was used for rating analysis. The visual analogue scale ratings and rating times for desire to void and pain induced by viscerosensory stimulation were analyzed separately by means of one-way repeated measure analysis of variance (ANOVA) with the prefill volumes (no-, low- and high-load) as the within-subjects factor. Two-tailed *post-hoc* pairwise comparison tests were performed to examine which pairs differed among different viscerosensory testing conditions. A Greenhouse-Geisser correction was used for sphericity when Mauchly's test indicated sphericity assumption was violated. Paired Student's *t*-test

was used for pairwise comparison of different interoceptive task conditions and differences were considered significant with $P < 0.05$.

DATA PROCESSING

Following the completion of each scan, acquired imaging data were exported to an offline workstation and preprocessed using Statistical Parametric Mapping (SPM) software (Wellcome Department of Cognitive Neurology, London, UK, version 8) running under the MATLAB environment (Mathworks, Natick, MA, release 13a). Data from each participant were first realigned (motion-corrected) using rigid body transformations [97], followed by slice-timing correction by temporally aligning all slices to the same reference time point (first slice). We chose to perform realignment first to minimize the effect of inter-slice movement [98]. This step was followed by co-registration of the functional images to the T1-weighted images, and spatial normalization to a standard stereotactic space (Montreal Neurological Institute, MNI, Quebec, Canada) [97]. The normalized functional images were smoothed with an isotropic Gaussian kernel of 8 mm at full width at half maximum. Finally, the data were intensity-normalized by dividing the time series of each voxel by its average intensity, and converting data to percent signal change units to improve the accuracy and test–retest reliability of ICA [99].

GROUP INDEPENDENT COMPONENT ANALYSIS

Data were decomposed into independent components (ICs) using spatial ICA. Spatial ICA applied to fMRI data aims to separate spatially independent patterns (referred to as spatial maps) from their linearly mixed BOLD signals (referred to as time courses) via maximization of mutual independence among components [42]. We used ICA to identify the networks because this multivariate, data-driven method requires no a priori hypothesis or model of brain activity. It simultaneously takes into account the relationships between all voxels, instead of, e.g., considering only the single region-dominant networks produced by seed-based correlations [100]. Additionally, ICA is capable of extracting scanner or physiological noise and motion artifacts from the dataset [101], and is not influenced by temporal sampling rates [102]. Finally, compared to seed-based approaches, ICA may offer better sensitivity to detect subtle differences among subjects [103], which is important for our study since interoceptive sensation varies among individuals [104-107].

Preprocessed time series were analyzed using the Group ICA of fMRI toolbox (GIFT) software package (Medical Image Analysis Lab, University of New Mexico, Albuquerque, New Mexico; version1.3 h). Data from all functional conditions were analyzed in one group ICA instead of four separate ICAs so that a tighter comparison between different task conditions could be performed without the added variability from separate ICA analyses [108]. The number of independent sources (i.e., optimal dimensionality of the ICs) was estimated using the GIFT dimensionality estimation tool based on the aggregated data using the minimum description length (MDL) criterion, modified to account for spatial correlation [109]. Note that there's no standard for selecting the number of ICA components. Too few means that essentially we are removing too much single subject variance while too many might segregate networks. MDL algorithm offers an estimate of the optimal number of ICs by

making a decision based upon the complexity or information content of the data. Briefly, this algorithm employs a subsampling scheme to obtain a set of effectively independent and identically distributed samples from the data and then applies the information-theoretic criteria to the sample set to estimate the number of informative components [109, 110]. MDL algorithm estimated the optimal dimensionality of the ICs in our dataset to be about 40 averaged across all participants (39.4 ± 6.15, mean ± SD). A two-step data reduction process was subsequently conducted [42]. First, fMRI data from individual participants were reduced to a lower dimensionality through subject-specific data reduction by principal component analysis with a standard economy-size decomposition. Next, reduced data from all participants were concatenated and reduced to one group and the independent group components were retained using the expectation-maximization algorithm. Statistical reliability of the IC decomposition (i.e., whether an IC has the tendency to split or merge with another IC) was determined by running the information maximization (infomax) algorithm [111] 100 times in the ICASSO software, a tool that is specialized for studying the reliability of ICA estimates by clustering and visualization [112]. Using this software, which is incorporated as part of the GIFT software package, the unmixing matrix was randomly initialized 100 times, then the infomax algorithm ran with each initialized unmixing matrix to extract specified number of ICs. The similarity between ICs from each condition was calculated by the absolute correlation. The agglomerative hierarchical clustering with average-linkage criterion was used for the clustering of the estimated ICs [112]. Finally, to identify subject-specific spatial maps and time courses, back-reconstruction was performed on the group components using a dual regression analysis (group ICA back-reconstruction approach number 3 (GICA-3) algorithm in the GIFT software package) [113].

Following previous studies, we used a methodical approach to identify ICs that were brain signals as opposed to noise or physiological artifacts [99, 108, 114-118]. First, the cluster quality index (Iq) from the ICASSO software was examined as the criterion to validate the reliability and stability of IC decomposition. The Iq ranges from 0 to 1 with values close to unity signifying that the corresponding component is reliably extracted, i.e., similar components are estimated at each condition of the ICA algorithm [116]. On the other hand, Iq values approaching zero implies that the likelihood that the component is randomly produced is higher [109]. ICs with the Iq value below 0.8 from 100 ICASSO repetitions were excluded from further analysis. Next, the spatial correlation of each IC's spatial map with a priori probabilistic maps of cerebrospinal fluid, white matter, and gray matter in MNI space as provided with SPM8 was assessed using GIFT spatial sorting. Components that showed high correlations with cerebrospinal fluid or white matter, or low correlations with gray matter indicating they might be artifacts or noise rather than hemodynamic change were identified and excluded from further analysis. Visual inspection of spatial patterns and frequency analysis of each IC spectra (i.e., time courses dominated by low-frequency fluctuations, see [119]) allowed additional components related to artifacts to be discarded. Identification of remaining ICs was performed through cross-correlation with reference standard network templates as well as knowledge from established brain networks described in previous studies [46, 99, 120-127]. Specifically, we performed a multiple spatial regression with a previously established and publicly available baseline set of reference components [99] as regressors of interest to identify equivalent ICs in our dataset. We chose reference networks from [99] to identify equivalent ICs in our dataset because for both datasets ICA was conducted using

the same software package (i.e., GIFT) following similar preprocessing procedure in SPM, while reference ICs from others studies such as [46, 124] used multivariate exploratory linear optimized decomposition into independent components (MELODIC) toolbox [128] in the FMRIB Software Library (FSL) [129, 130]. Although unlike our task-derived ICs, reference networks from [99] are derived from the resting-state data, ICA networks have been consistently and reliably identified in both the resting state [100, 122] as well as task activation fMRI studies [46, 124, 131, 132] affirming that similar networks, with strong spatial correspondence to the resting state, could also be elicited using task paradigms [45].To display voxels relevant to a particular IC, we normalized back-reconstructed spatial maps of each IC into *z*-score [42, 128]. The normalized spatial maps of *z*-scores of individual subject were averaged together across the four functional conditions, and the averaged maps of *z*-scores were plotted as t-statistics, thresholded at $t > \mu + 4\sigma$ (following the justification described in appendix B in [99]). Component anatomical locations and Brodmann's areas (BA) were determined using the cytoarchitectonic probability maps as implemented in the SPM Anatomy Toolbox [133].

TASK-RELATED MODULATIONS OF NETWORKS

In order to assess the degree of task relevance of each ICA component, regression analysis of component time courses was conducted. First a design matrix of task regressors for each viscerosensory condition was constructed using SPM8. The design matrices represented the onset of each task condition, convolved with a box-car hemodynamic response function (HRF; [134]). For the NO-PREFILL WARM and NO-PREFILL COLD conditions, a design matrix of four regressors (i.e., infusion, filled state, rating after filled, and drainage), and for the LOW-PREFILL WARM and HIGH-PREFILL WARM conditions, a design matrix of six regressors (i.e., infusion, filled state, rating after filled, drainage, emptied state, and rating after emptied) were created. For each viscerosensory task, the component time courses were temporally sorted according to the strength of correlation between the component time courses and the time course of each of these events as embodied in the design matrices. This procedure led to a set of regression coefficients (termed β-weights) for each regressor associated with each participant. These weights, which represented the degree of synchrony between IC time courses and reference time courses, were used to assess engagement of each IC during different task conditions [117, 118]. Positive and negative β-weights at one task condition relative to another indicate positive and negative correlation with task-related activity in the IC. Furthermore, a greater absolute value of the β-weight usually indicates a greater engagement (task-related up-modulation if the sign is positive) or disengagement (task-related down-modulation for negative bs) of an IC [118]. Two-tailed one-sample Student's *t*-test against zero was performed on β-weights separately for each condition ($P < 0.05$). These *P*-values were not corrected for the total number of comparisons because these β-weights were not all independent between trials (e.g., infusion vs. drainage) in the same component or between components for the same condition [118]. In addition to the β-weights statistics, we computed the event-related averages for each task-related ICs over a default window of 30 s as implemented in the GIFT software package. These event-related averages represent their associated IC activation level over the course of a typical HRF during a task.

FUNCTIONAL NETWORK CONNECTIVITY

Temporal correlations among the time series of the task-related ICs were assessed using the FNC toolbox (Medical Image Analysis Lab, University of New Mexico, Albuquerque, New Mexico; version 2.3). The ICA algorithm assumes synchronicity between the time courses of the responses in cortical areas within one IC [114]. Though the ICs are maximally spatially independent, significant temporal correlations can exist between them [42]. To examine this, a constrained maximal time-lagged correlation method was used. Pearson's correlation between the time course of each task-related IC pairs was computed as in [43] with maximal lag set to 4 s (2*TR, TR = 2 s). Allowing lag between time courses is important to account for HRF shape variations among brain regions as well as among different subjects, although the source of this lag is still debatable [135]. Prior to computing correlations, networks' time courses were filtered using a band pass Butterworth filter with cut-off frequencies at 0.017 and 0.24 Hz to suppress the very low and very high frequencies, respectively [108]. The maximum correlation and the corresponding lag values were subsequently calculated for every subject and separately for each task condition. Correlations were normalized using Fisher's transformation [z = arctanh (r)] and the robustness of maximum lagged correlation between time course pairs was tested. To determine the significant differences between task conditions, paired Student's t-test was performed. For all FNC analyses, the cut-off P-value was set at 0.05, false discovery rate (FDR)-corrected for multiple comparisons [136].

RESULTS

RATING SENSATIONS DURING THE SCAN

Statistical analysis of the rating sensations during the scan (**Table 1**) by means of ANOVA revealed a significant effect of adding 100 ml warm saline to the prefill volume on desire to void sensation [$F(2, 24) = 128.11$, $P < 0.001$, $\eta_p^2 = 0.914$]. *Post-hoc* pairwise comparisons indicated that the mean desire to void rating after infusion was lower for NO-PREFILL WARM condition than for LOW-PREFILL WARM [$t(12) = 2.67$, $P = 0.02$], and HIGH-PREFILL WARM [$t(12) = 18.50$, $P < 0.001$]. There was a significant difference in the mean desire to void rating between LOW-PREFILL WARM and HIGH-PREFILL WARM [$t(12) = 11.594$, $P < 0.001$] (**Figure 2**). Despite having base level of zero (i.e., empty UB) for NO-PREFILL WARM and NO-PREFILL COLD conditions, a paired Student's t-test indicated that subjective desire to void sensation after infusion of 100 ml cold saline was significantly greater than desire to void sensation after infusion of 100 ml warm saline [$t(12) = 5.60$, $P < 0.001$]. There was no significant effect of prefill volume on pain after infusion of 100 ml warm saline in any prefill conditions [Greenhouse-Geisser corrected, $F(1, 15) = 4.49$, $P = 0.056$, $\eta_p^2 = 0.272$]. Similarly, no significant effect of prefill volume was found on either desire to void or pain rating times [$F(2, 24) = 0.801$, $P = 0.460$, $\eta_p^2 = 0.063$, and $F(2, 24) = 0.832$, $P = 0.447$, $\eta_p^2 = 0.065$, respectively].

Table 1 Rating values for desire to void and pain sensations during the fMRI scan

Viscerosensory condition		Rating value	Rating time
NO-PREFILL WARM	Desire to void after infusion	1.47 ± 1.07	5.68 ± 0.64 s
	Pain after infusion	0.55 ± 0.31	4.83 ± 0.78 s
LOW-PREFILL WARM	Desire to void after infusion	2.79 ± 1.87	5.92 ± 0.67 s
	Pain after infusion	0.53 ± 0.27	5.27 ± 0.87 s
	Desire to void after Drainage	1.72 ± 1.39	5.62 ± 0.60 s
	Pain after Drainage	0.55 ± 0.34	5.33 ± 0.71 s
HIGH-PREFILL WARM	Desire to void after infusion	8.17 ± 1.01	5.90 ± 0.68 s
	Pain after infusion	0.99 ± 0.75	5.12 ± 1.02 s
	Desire to void after Drainage	5.41 ± 1.06	6.07 ± 0.62 s
	Pain after Drainage	0.59 ± 0.31	5.57 ± 0.75 s
NO-PREFILL COLD	Desire to void after infusion	5.46 ± 2.44	5.69 ± 0.95 s
	Pain after infusion	1.56 ± 1.63	5.45 ± 0.81 s

Paired Student's *t*-test showed that the mean desire to void rating after drainage was significantly higher for HIGH-PREFILL WARM compared to LOW-PREFILL WARM condition [$t(12) = 10.191$, $P < 0.001$]. The desire to void ratings after drainage were also significantly different from desire to void rating after infusion for the LOWPREFILL WARM [$t(12) = 2.66$, $P = 0.021$], and HIGHPREFILL WARM [$t(12) = 6.695$, $P < 0.001$]. There was no significant difference in the mean rating time for desire to void after infusion versus after drainage for the LOWPREFILL WARM [$t(12) = 1.592$, $P = 0.137$], or the HIGHPREFILL WARM [$t(12) = 0.725$, $P = 0.482$]. Similarly, there was no statistically significant difference in pain rating value or rating time between any pairs across the four task conditions.

In post-scan interviews, all participants reported following the suggested strategy of focusing on the sensations during stimulus administration and waiting for the appearance of the visual analogue scale on the screen to perform the rating. There was no report of discomfort or painful sensations associated with the supine-lying position, length of the scanning period, or the use of the stabilization foam pads around their head and neck areas. A potential reason that pain was not a true zero here might be due to the fact that we used an analogue visual scale with two-digit decimal accuracy. We also used a custom-made response box [96] with a manipulandum instead of a commercial button box. Thus getting a true zero was difficult using this analogue scale and the said custom-made rating device.

Furthermore, prior to fMRI scans participants were evaluated clinically (voiding diary) and urodynamically (maximum cystometric capacity, maximum detrusor pressure, desire to void, etc.). The maximum cystometric capacity, which reflect the maximum functional UB volume, and the prefilled UB volume for strong desire to void, which was used for profiling prior to the HIGH-PREFILL WARM condition, were on average 658.7 ± 138.3 ml, and 446.7 ± 110.6 ml (mean ± SD), respectively (**Supporting Table 1**).

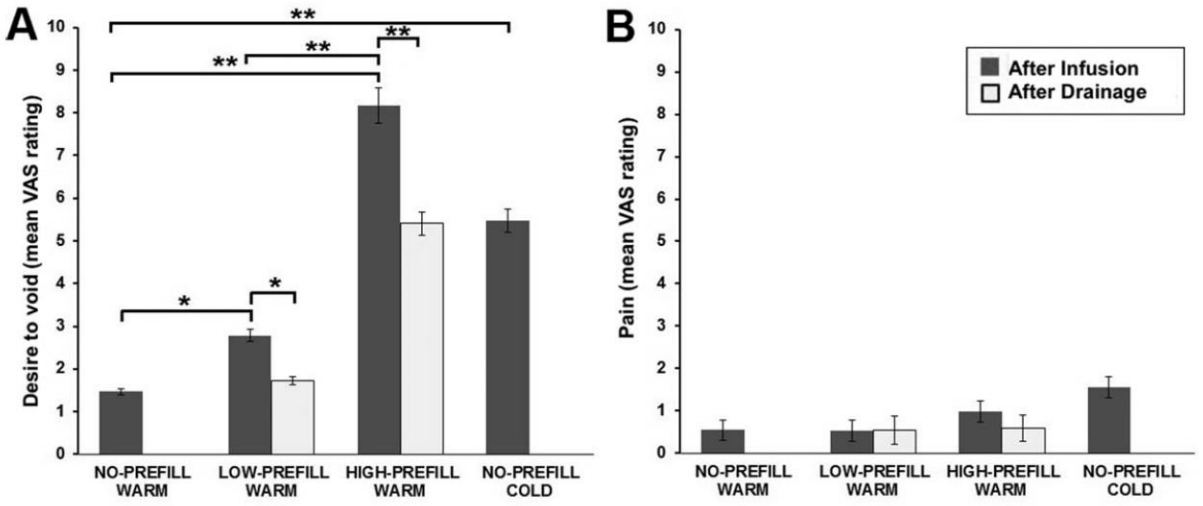

Figure 2 Summary of online ratings for pain and desire to void sensations averaged across all participants. (A) Group analysis of desire to void sensation ratings demonstrated significant difference between NO-PREFILL, LOW-PREFILL and HIGH-PREFILL conditions after infusion. There was also a significant difference in desire to void ratings between infusion and drainage for the LOW-PREFILL and HIGH-PREFILLWARM. (B) Group analysis of pain ratings showed no statistically significant difference between any pairs across the four task conditions. *$P < 0.05$, **$P < 0.001$.

NETWORK MODULATIONS DURING VISCERAL INTEROCEPTION

Out of 40 ICs (**Supporting Figure 1**), we identified 25 components to be brain networks and discarded the rest as physiological artifacts, head movements, scanner noise, or mixture of brain signals and artifacts. Specifically, to identify equivalent ICs in our dataset to the standard references, we performed a multiple spatial regression with a previously established baseline set of ICA components as regressors of interest [99]. Subsequently, we tested the significance level of β-weights for the 25 networks (i.e., non-artifactual ICA components). For ICs surviving the uncorrected $P < 0.05$, we selected those that were among the top five rank ordered components for "infusion," "filled," "drainage" or "emptied" trials separately for each viscerosensory stimulation condition and attained task-relevant networks for the corresponding condition. In **Figure 3–6**, (a) the task-related components' spatial maps, (b) associated β-weights, and (c) related event averages of task trials as computed from the component time courses are presented for the NO-PREFILL WARM, NO-PREFILL COLD, LOW-PREFILL WARM, and HIGHPREFILL WARM conditions, respectively. Detailed information of component spatial map including the main regions of positive activation, BA, number of voxels, peak activation *t*-value, and MNI coordinates are listed in the **Table 2**. The group mean and standard deviation of β-weights, and corresponding uncorrected *P*-values from one-sample *t*-tests for task-related ICs are presented in **Table 3** and **Table 4**, separately for each condition.

ICs 30 and 31 involve the dorsolateral PFC and posterior parietal cortices (similar to the reference components 34 and 60 in [99], with multiple regression values of 0.34 and 0.61, respectively). These reference components were identified in [99] as central executive networks [127, 137]. IC 35 matched the so-called the default mode brain network reference components from [99] (reference component 53, multiple regression value: 0.46, reference component 25, multiple regression value: 0.29, and reference component 68, multiple regression value: 0.17) with clusters in the medial PFC, ACC, the

precuneus/ posterior cingulate cortex, bilateral parietal lobules and the inferior temporal gyri [138, 139]. IC 33 showed the strongest overlap with reference component 50 from [99] (multiple regression value: 0.16), which comprises more posterior parts of the default mode network involving the posterior midline structures of the precuneus/posterior cingulate cortex and inferior parietal lobules [139, 140]. IC 16 involves the anterior insula/frontal opercula extending to the bilateral IFG (**Table 2**). Reference component 55 from [99], which is classified as an ACC/insular network in that publication, showed the strongest overlap with this network (multiple regression value: 0.28). This reference component for the ACC/insular network also partially matched a second component (IC 26) in our dataset covering bilateral posterior insula infringing toward putamen, and IFG in addition to the ACC (multiple regression value: 0.08). IC 11 encompassing the bilateral striatum, insula, and thalamus, showed strong overlap with the reference component 21 from [99] (multiple regression value: 0.71). Reference component 21 from [99] is termed basal ganglia network in that publication with activation focused in the putamen and pallidum [124, 141]. IC 27 involving the bilateral temporal-parietal junction (TPJ) including the supramarginal and superior temporal cortex and precuneus, showed strong similarity to the reference component 71 focused at the TPJ ([99]; multiple regression value: 0.55), as well as the reference component 72 centered in the central and anterior precuneus ([99]; multiple regression value: 0.14). IC 2 includes the ACC (small dorsal, more ventral, i.e., pregenual and subgenual ACC) and the adjacent ventromedial PFC, IFG, as well as the ventral sections of the bilateral caudate (**Table 2**). This IC showed strong overlap with the anterior default mode network reference component from [99] (i.e., component 25; multiple regression value: 0.38). It resembles a network termed self-referential network in [121, 125]. IC 3 is composed of the bilateral amygdala, parahippocampal gyri and midbrain. IC 22 also involves the bilateral hippocampi and parahippocampal gyri as well as the thalamus, midbrain and brainstem. IC 24 contains the bilateral thalamus, and brainstem. ICs 9 and 12 cover the bilateral cerebellum. The latter ICs did not strongly match any of the reference component from [99] since no cerebellar/brainstem components were included in the list of 28 reference components.

NETWORK MODULATIONS DURING THE NO-PREFILL WARM CONDITION

Accounting for the largest positive β-weight during both “infusion” and “filled” phases of the NO-PREFILL WARM condition was IC 30 (**Figure 3**, **Table 3**). IC 26 was the second most up-regulated network during both “infusion” and “filled” after IC 30. During the “drainage,” IC 30 still showed large positive up-regulation, but its correlation with the drainage task was weaker than IC 26. Additionally, ICs 35 and 22 showed significant positive correlation during the “drainage.” The other highly-rank networks include ICs 31 and 27. These networks both displayed positive up-regulation during “infusion” but neither correlates with the “drainage.”

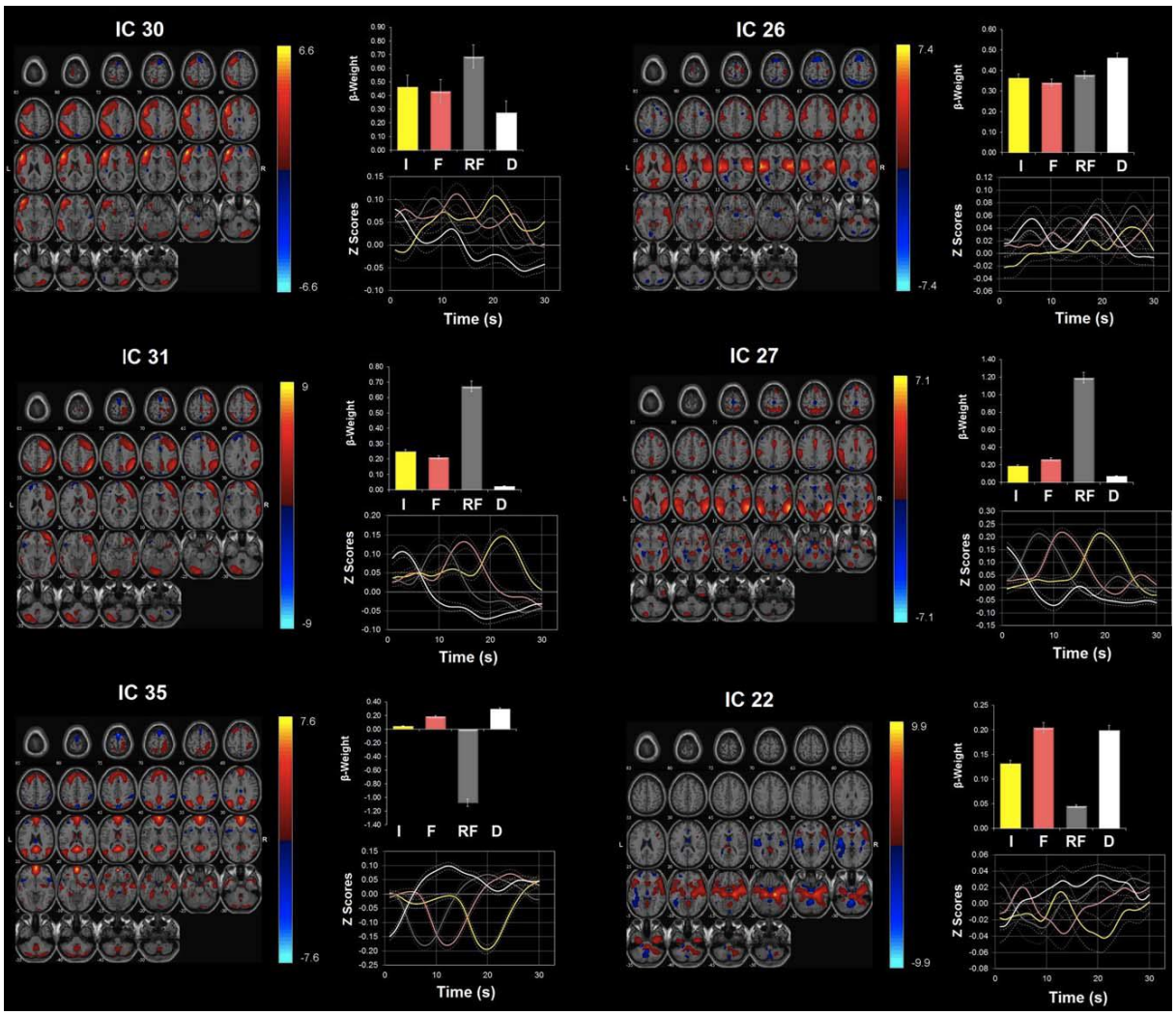

Figure 3 Network modulations during the NO-PREFILL WARM condition. Six ICA components showed statistically significant ($P < 0.05$, uncorrected) activity increases with the NO-PREFILL WARM condition: ICs 30, 26, 31, 27, 35, and 22. All were identified from ICA with regions with positive (warm color) and negative (cool color) signal change shown on the MNI T1 template (right = right). The color bar indicates *t* values. For each ICA component, the β-weights and event averages of I (infusion), F (filled), RF (rating after filled), and D (drainage) trials are demonstrated.

NETWORK MODULATIONS DURING THE NO-PREFILL COLD CONDITION

Similar to the NO-PREFILL WARM condition, the highest positively task-modulated network during both "infusion" and "filled" trials was IC 30 (**Figure 4**, **Table 4**). It was closely followed by IC 31, as well as IC 27. IC 26 was the next highly-correlated network during the "infusion" but it was not significantly modulated during the "filled" phase. In its place, IC 16 showed significant task-correlation during "infusion" as well as "filled" phases. The other network that was highly active during the "filled" phase is IC 24. During the "drainage," ICs 26 and 24 showed significant task-related modulation.

NETWORK MODULATIONS DURING THE LOW-PREFILL WARM CONDITION

Four networks show significant task-related modulation during different phases of the LOW-PREFILL WARM condition (**Figure 5**, **Table 5**): ICs 11, 2, 3, and 33. Specifically, IC 11 showed significant up-regulation during the "infusion," "drainage" and "emptied" trials. ICs 2 and 3 were both highly correlated with the "filled" and "emptied" trials. IC 33 was active only during the "drainage."

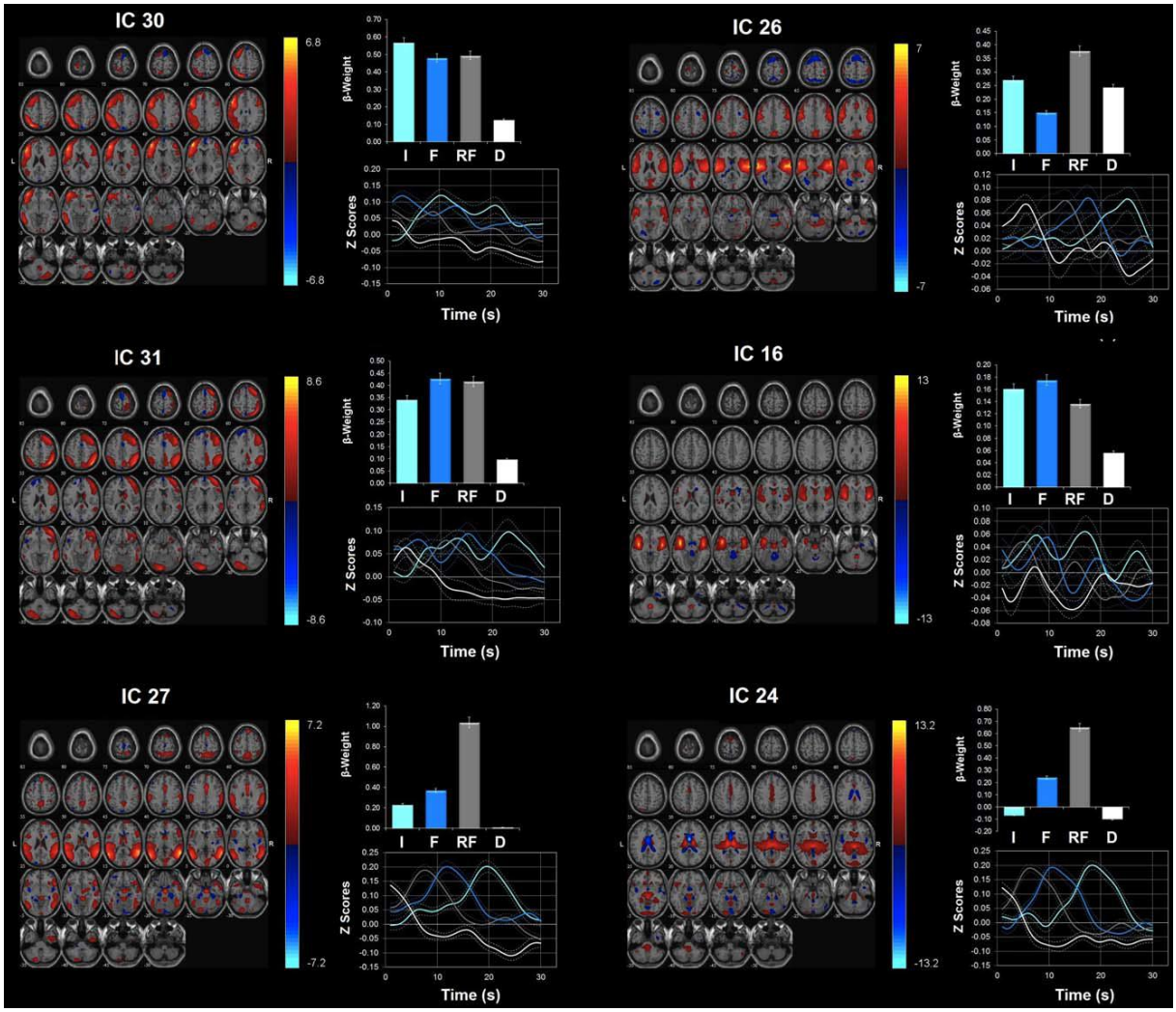

Figure 4 Network modulations during the NO-PREFILL COLD condition. Six ICA components showed statistically significant ($P < 0.05$, uncorrected) activity increases with NO-PREFILL COLD condition: ICs 30, 26, 31,16, 27, and 24. All were identified from ICA with regions with positive (warm color) and negative (cool color) signal change shown on the MNI T1 template (right = right). The color bar indicates *t* values. For each ICA component, the β-weights and event averages of I (infusion), F (filled), RF (rating after filled), and D (drainage) trials are demonstrated.

NETWORK MODULATIONS DURING THE HIGH-PREFILL WARM CONDITION

In addition to the four networks that showed significant task-related modulation during different trials of the LOW-PREFILL WARM condition, i.e., ICs 11, 2, 3, and 33, three additional networks were significantly upregulated during the HIGH-PREFILL WARM condition (**Figure 6**, **Table 6**). These extra components included ICs 9, 12, and 24. During the "infusion," ICs 11, 3, and 12 were highly

modulated. During the "filled" phase, IC 24 becomes significantly active in addition to ICs 11 and 3. During the "drainage," ICs 11 and 33 were up-regulated as well as another cerebellar component, IC 9. ICs 2 and 3 were only up-regulated network during the "emptied" trials.

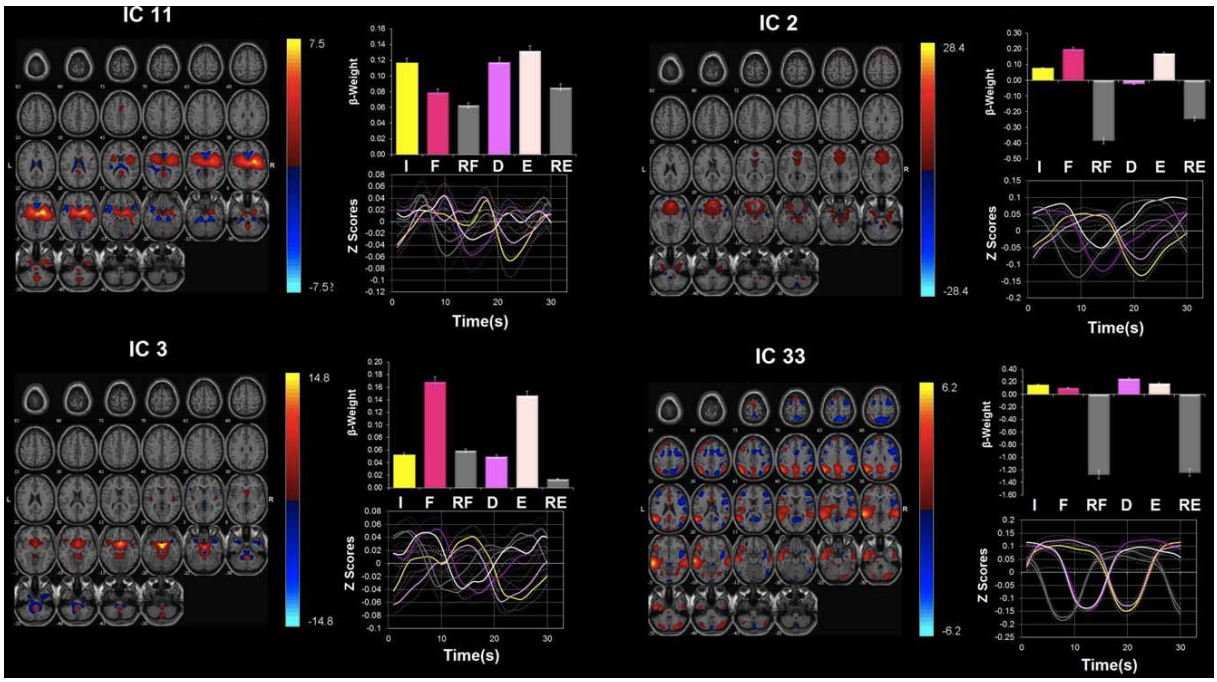

Figure 5 Network modulations during the LOW-PREFILL WARM condition. Four ICA components were identified as statistically significant ($P < 0.05$, uncorrected) upregulated during the LOWPREFILL WARM condition: ICs 11, 2, 3, and 33. All were identified from ICA with regions with positive (warm color) and negative (cool color) signal change shown on the MNI T1 template (right = right). The color bar indicates *t* values. For each ICA component, the β-weights and event averages of I (infusion), F (filled), RF (rating after filled), and D (drainage), E (emptied), and RE (rating after emptied) trials are demonstrated.

FUNCTIONAL NETWORK CONNECTIVITY DURING VISCERAL INTEROCEPTION

For each viscerosensory stimulation condition, the top three networks that were highly modulated by its task condition were selected for FNC analysis. Seven task-relevant networks were thus retained for this purpose: ICs 2, 3, 11, 26, 27, 30, and 33. The maximum lagged correlation between these task-related networks was computed for each subject and task condition following the procedures described in [43]. The correlation was then examined between all pair-wise combinations where the number of combinations of seven components, taken two at a time resulted in 21 possible combinations. For the correlation pairs, Student's *t*-test was conducted at $P = 0.05$, FDR-corrected for multiple comparison. In **Figure 7**, the matrices of mean FNC correlation, and the corresponding *t*-test results for each condition are shown in the lower and upper half of matrices, respectively. The black asterisk in each correlation matrix identifies the correlation pairs that survived the *t*-test. The time lag pairs are also shown in **Figure 8** with arrows representing significant FNC correlation between components ($P < 0.05$, FDR-corrected). For demonstration purpose, the lag time between the

connected networks is shown by the direction of the arrow. The averaged time lag values for the four viscerosensory stimulation conditions are provided in the **Supporting Figure 2**.

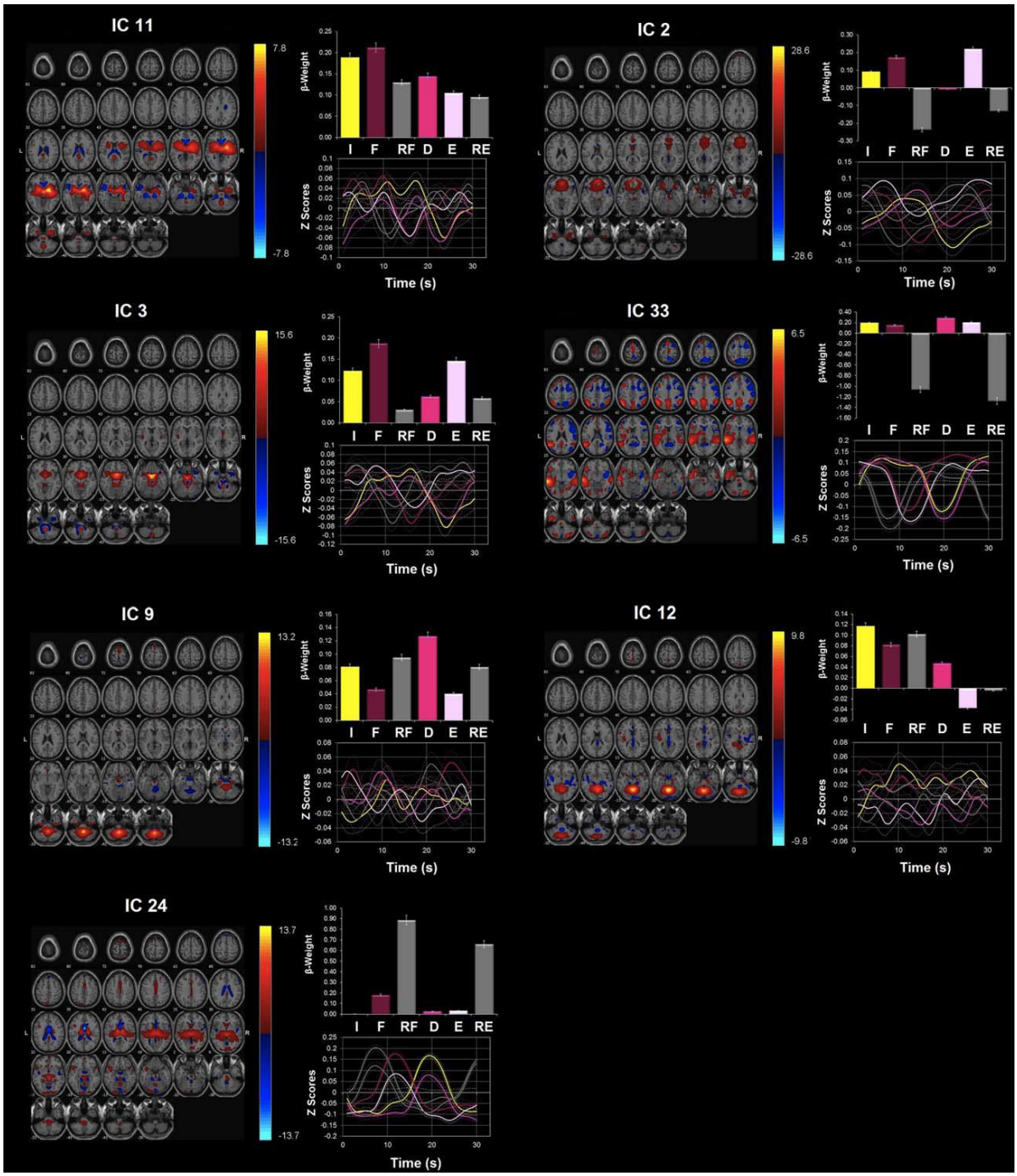

Figure 6 Network modulations during the HIGH-PREFILL WARM condition. Seven ICA components were highly upregulated during the HIGH-PREFILL WARM condition ($P < 0.05$, uncorrected): ICs 11, 2, 3, 33, 9, 12, and 24. All were identified from ICA with regions with positive (warm color) and negative (cool color) signal change shown on the MNI T1 template (right = right). The color bar indicates *t* values. For each ICA component, the β-weights and event averages of I (infusion), F (filled), RF (rating after filled), and D (drainage), E (emptied), and RE (rating after emptied) trials are demonstrated.

To determine which FNC between network pairs are significantly different among four interoceptive conditions, paired *t*-tests were conducted at FDR-corrected threshold level of $P = 0.05$. The results are

shown in **Figure 9**A,B, corresponding to significant differences that were found between the NO-PREFILL WARM and LOW-PREFILL WARM condition pair, and the NO-PREFILL WARM and HIGH-PREFILL WARM condition pair, respectively. Matrices of mean correlation difference and *t*-value resulting from paired *t*-tests for network pairs are shown in **Figure 10**. The asterisk indicates those surviving the paired *t*-test. The corresponding values of the time lag differences for the network pairs are supplied in the **Supporting Figure 3**.

DISCUSSION

In this study, we used a multivariate approach, namely ICA, to study brain networks [44] (i.e., ICA components) modulated by visceral interoception from the UB as a representative internal organ. Results show that the innocuous (non-painful) temperature stimulation of the UB mucosa activated ICA components encompassing the bilateral insula, ACC, dorsolateral PFC and posterior parietal cortex, thalamus, and TPJ. The distention pressure on the viscera (i.e., UB fullness), on the other hand, engaged the bilateral striatum, insula, ACC, ventromedial PFC, the amygdalo-hippocampi and parahippocampal gyri, thalamus, the posterior midline structures of the precuneus/posterior cingulate cortex and the bilateral inferior parietal lobules, and cerebellar components. Significant differences in FNC ($P < 0.05$, FDR-corrected) were found between the insula, ACC, and amygdalo-hippocampus, between the insula, ACC, and ventromedial PFC, and between the ventromedial PFC and TPJ as the distention pressure on the viscera increased confirming that functional interactions between components changed as a function of viscerosensory condition. In the following we discuss the significance of these new findings.

Table 2 Peak activations of the ICA component spatial maps[a]

IC	Brain region	Cluster size (voxels)	t_{max}	MNI coordinates			Cytoarchitectonic Brodmann area (Probability, if available)
				x	y	z	
IC 2 (0.98)	Right anterior cingulate cortex	1944	44.32	6	32	0	
	Right inferior frontal gyrus	same cluster	33.45	27	29	–15	
	Left caudate nucleus	same cluster	22.47	–6	17	0	
	Left middle orbital gyrus	same cluster	16.94	–21	32	–21	
	Right parahippocampal gyrus	57	13.65	21	–1	–27	Hipp (EC) (90%)
IC 3 (0.97)	Right parahippocampal gyrus	1068	21.43	9	2	–18	Hipp (EC) (20%)
	Right olfactory cortex	same cluster	28.42	3	11	–9	
	Left caudate nucleus	same cluster	27.44	–6	8	6	
	Right amygdala	same cluster	15.66	24	–1	–12	Amyg (SF) (80%)
IC 9 (0.97)	Right cerebellum	2140	31.32	12	–46	–36	
	Left cerebellum	same cluster	30.33	–21	–46	–48	Lobule VIIIb (Hem) (52%)
IC 11 (0.98)	Right insula lobe	3979	50.75	39	–7	–6	Insula (Id1) (20%)
	Right thalamus	same cluster	33.50	12	–16	3	Th-Prefrontal (84%)
	Left putamen	same cluster	31.22	–30	–1	9	
IC 12 (0.97)	Left cerebellum	2741	32.09	–18	–70	–30	Lobule (VI (Hem) (98%)
	Right cerebellum	same cluster	30.57	12	–49	–24	Lobule V (69%)
IC 16 (0.96)	Left insula lobe	1549	26.19	–39	–5	5	
	Left inferior frontal gyrus	same cluster	22.62	–51	23	0	Area 45 (40%)
	Left Rolandic operculum	same cluster	20.98	–54	5	6	OP 4 (40%)
	Right insula lobe	1026	31.90	45	–1	0	OP 3 (10%)

IC	Brain region	Cluster size (voxels)	t_{max}	MNI coordinates			Cytoarchitectonic Brodmann area (Probability, if available)
				x	y	z	
	Right inferior frontal gyrus	same cluster	18.43	48	20	–6	Area 45 (10%)
IC 22 (0.97)	Right fusiform gyrus	3575	34.33	33	–37	–21	
	Right parahippocampal gyrus	same cluster	32.66	24	–4	–33	Hipp (EC) (100%)
	Left inferior frontal gyrus	same cluster	26.66	–48	26	–9	Area 45 (20%)
	Left caudate nucleus	70	13.74	–12	19	5	
IC 24 (0.97)	Left thalamus	2314	36.22	–15	–31	3	
	Right thalamus	same cluster	24.69	6	–16	12	
	Pons	86	13.54	–9	–25	–33	
IC 26 (0.95)	Right insula lobe	2568	44.03	39	–19	12	Insula (Ig2) (80%)
	Right Rolandic operculum	same cluster	31.82	51	–1	6	OP 4 (30%)
	Right putamen	same cluster	23.58	30	–7	12	OP 3 (20%)
	Left superior temporal gyrus	2052	24.91	–60	–28	6	
	Left Rolandic operculum	same cluster	24.04	–48	–16	12	OP 1 (10%)
	Left insula lobe	same cluster	22.91	–36	–13	6	Insula (Ig2) (50%)
	Right middle cingulate cortex	216	22.90	6	29	30	
	Right anterior cingulate cortex	same cluster	8.83	15	38	21	
IC 27 (0.95)	Left middle temporal gyrus	1820	28.07	–45	–52	12	IPC (PGa) (30%)
	Left inferior parietal lobule	same cluster	26.29	–51	–25	36	IPC (PFt) (80%)
	Right middle temporal gyrus	1661	44.67	48	–55	12	IPC (PGp) (20%)
	Right supramarginal gyrus	same cluster	29.67	63	–37	24	IPC (PF) (100%)
	Left precuneus	307	22.47	–9	–52	48	SPL (5M) (20%)
IC 30 (0.92)	Left precentral gyrus	4155	38.75	8	–57	18	Area 44 (50%)
	Left inferior frontal gyrus	same cluster	27.39	–42	35	15	Area 45 (60%)
	Left middle orbital gyrus	same cluster	25.87	–42	50	–3	
	Right precentral gyrus	454	14.45	–4	45	–9	Area 44 (40%)
	Right inferior frontal gyrus	same cluster	18.22	57	20	9	Area 45 (60%)
	Right Rolandic operculum	same cluster	11.37	57	–13	18	OP 4 (70%)
	Right cerebellum	338	19.51	36	–70	–36	Lobule VIIa (Hem) (60%)
	Left inferior temporal gyrus	121	19.83	–54	–40	–15	
	Left superior medial gyrus	100	13.41	–9	44	42	
IC 31 (0.92)	Right middle orbital gyrus	1967	29.04	36	50	–6	
	Right superior medial gyrus	same cluster	25.04	12	32	45	
	Right middle frontal gyrus	same cluster	24.63	36	53	3	
	Left cerebellum	1179	25.37	–39	–76	–30	Lobule VIIa (Hem) (98%)
	Right inferior parietal lobule	1149	31.99	48	–55	45	IPC (PGa) (50%)
	Right postcentral gyrus	same cluster	13.23	39	–31	51	Area 3b (100%)
	Left inferior parietal lobule	408	18.99	–42	–58	48	hIP1 (50%)
IC 33 (0.93)	Left inferior parietal lobule	2157	21.37	–51	–52	45	IPC (PFm) (60%)
	Right superior temporal gyrus	420	19.15	60	–31	3	
	Right precuneus	361	23.68	3	–55	33	SPL (7A) (10%)
	Left posterior cingulate cortex	same cluster	20.81	–6	–52	30	
	Right angular gyrus	174	17.49	45	–55	36	IPC (PGa) (60%)
	Right middle frontal gyrus	same cluster	9.75	36	35	36	IPC (PFm) (70%)
IC 35 (0.90)	Left mid orbital gyrus	1889	42.95	–6	65	–6	
	Left superior medial gyrus	same cluster	30.18	–3	71	3	
	Left anterior cingulate cortex	same cluster	17.89	–3	47	6	
	Right superior frontal gyrus	same cluster	15.49	24	38	51	Area 5 (10%)
	Left precuneus	962	29.50	0	–58	30	SPL (7A) (10%)
	Right cuneus	same cluster	26.77	12	–61	21	
	Left cerebellum	679	19.90	–12	–64	–42	Lobule VIIIb (Hem) (30%)
	Right superior parietal lobule	482	16.18	18	–49	63	SPL (5L) (80%)
	Right parahippocampal gyrus	417	26.54	30	–25	–21	Hipp (SUB) (80%)
	Right angular gyrus	357	31.10	54	–64	30	IPC (PGp) (90%)
	Left superior parietal lobule	355	16.47	–27	–76	45	IPC (PGp) (20%)

[a]The MNI (Montreal Neurological Institute) coordinates show the coordinates of the peak voxels with negative *x* coordinates refer to left hemisphere activations.
Brodmann's area as indicated by the cytoarchitectonic maximum probability map using the SPM-Anatomy toolbox developed by Eickhoff et al. [133]. The quality index (Iq) associated with each component is listed in parentheses next to the component number.

NETWORK MODULATION DURING INNOCUOUS TEMPERATURE STIMULATION OF MUCOSA

In the NO-PREFILL WARM condition, ICs 26, 30 and 31 and 27 demonstrated increased activity during infusion. In the NO-PREFILL COLD condition, almost identical components showed increased activity during infusion. COLD filling also significantly activated ICs 16 and 24. The majority of the activated components during the NOPREFILL conditions including ICs 26, 16, 30 and 31 involving the insula, ACC, and dorsolateral PFC are proposed to be responsible for detection of salient targets and task-appropriate attentional focus [142]. ICs 16 and 26 anchored by the bilateral insula and ACC, have been shown by several neuroimaging studies to play a crucial role in (a) attending to homeostatically relevant stimuli [13, 21, 23], (b) facilitating interactions of other large-scale intrinsic networks involved in externally oriented attention and internally oriented cognition [143, 144], (c) integrating interoceptive and exteroceptive signals [49, 145], and (d) engendering subjective feeling states [146-149].

Table 3 Temporal sorting for I (infusion), F (filled), RF (rating after filled) and D (drainage) trials of the NO-PREFILLWARM condition

	β-weights: Mean ± SD				One-sample *t*-test: *P*-value[a]			
IC	I	F	RF	D	I	F	RF	D
IC 30	0.46 ± 0.31	0.43 ± 0.33	0.69 ± 0.54	0.27 ± 0.34	0.000[b]	0.000[b]	0.00a[b]	0.014[b]
IC 26	0.36 ± 0.27	0.34 ± 0.27	0.38 ± 0.43	0.46 ± 0.33	0.000[b]	0.001[b]	0.008[b]	0.000[b]
IC 31	0.25 ± 0.35	0.21 ± 0.37	0.67 ± 0.41	0.03 ± 0.32	0.026[b]	0.060	0.000[b]	0.784
IC 27	0.19 ± 0.30	0.27 ± 0.41	1.19 ± 0.57	0.07 ± 0.35	0.042[b]	0.037[b]	0.000[b]	0.454
IC 35	0.05 ± 0.41	0.19 ± 0.33	–1.08 ± 0.51	0.30 ± 0.30	0.693	0.061	0.000[b]	0.004[b]
IC 22	0.13 ± 0.25	0.20 ± 0.36	0.05 ± 0.36	0.20 ± 0.17	0.083	0.066	0.655	0.001[b]

[a]One-sample *t*-test was performed to determine whether the β-weights are statistically different from zero. All *P*-values were uncorrected because these β-weights were not independent between trials for the same IC or between ICs for the same trial.
[b]$P < 0.05$.

Table 4 Temporal sorting for I (infusion), F (filled), RF (rating after filled) and D (drainage) trials of the NO-PREFILL COLD condition

	β-weights: Mean ± SD				One-sample *t*-test: *P*-value[a]			
IC	I	F	RF	D	I	F	RF	D
IC 30	0.57 ± 0.22	0.48 ± 0.51	0.49 ± 0.46	0.12 ± 0.29	0.000[b]	0.006[b]	0.002[b]	0.143
IC 31	0.34 ± 0.27	0.43 ± 0.38	0.42 ± 0.45	0.10 ± 0.25	0.001[b]	0.002[b]	0.006[b]	0.191
IC 26	0.27 ± 0.35	0.15 ± 0.57	0.38 ± 0.56	0.24 ± 0.33	0.016[b]	0.357	0.032[b]	0.021[b]
IC 27	0.23 ± 0.28	0.37 ± 0.35	1.04 ± 0.45	0.01 ± 0.33	0.013[b]	0.002[b]	0.000[b]	0.921
IC 16	0.16 ± 0.21	0.18 ± 0.22	0.14 ± 0.30	0.06 ± 0.11	0.015[b]	0.012[b]	0.125	0.101
IC 24	–0.07 ± 0.25	0.24 ± 0.26	0.65 ± 0.32	–0.10 ± 0.16	0.345	0.006[b]	0.000[b]	0.048[b]

[a]One-sample *t*-test was performed to determine whether the β-weights are statistically different from zero. All *P*-values were uncorrected because these β-weights were not independent between trials for the same IC or between ICs for the same trial.
[b]$P < 0.05$.

A recent meta-analytic clustering of data obtained from the BrainMap database revealed that insula can be parcellated to the anterior, and the posterior clusters [150]. The anterior cluster, which is characterized by an attentional pattern of connectivity with frontal, cingulate, parietal, cerebellar areas, is more homogeneous in comparison to the posterior cluster that is characterized by a more local connectivity pattern with connections to sensorimotor, temporal and posterior cingulate regions [150].

This finding supports the view that the network to which the anterior insula belongs is related to saliency detection. Similar meta-analytic clustering of cingulate cortex showed extensive co-activations within the cingulate cortex and the insula further supporting the view that the cingulate cortex and the insula form a saliency network devoted to the integration of internal (e.g., homeostatic) and the external (e.g., sensory) information [151]. According to the interoceptive model [2, 15, 17, 146], different sections of the insula are involved in distinctive and sequential neural processing of interoception from sensing the homeostatic condition of the body to the integration of motivational, hedonic, and social conditions [152]. It is proposed that the raw interoceptive signals such as those coming from viscerosensory stimulations and pain, are first mapped into a first-order mapping structure in posterior insula (i.e., primary interoceptive cortex) with additional regions—the so-called second-order regions such as the anterior insula, the ACC and the PFC become progressively involved [2, 15, 17, 146] as subjective awareness of feeling (e.g., desire to void), hedonic information, contextual motivational, and volitional control of related actions (e.g., voiding) emerges [5, 153]. The present ICA results dovetail with this model. In the NO-PREFILL WARM condition, the visceral afferents mapped the UB filling state to the posterior insula (the primary interoceptive cortex in IC 26) but did not ascend further to the anterior section of insula (i.e., no activation of IC 16) as the accumulated volume in the UB did not surpass the threshold of the so-called “first desire to void” [86]. This corresponded well with the fact that subjects could not discern the UB fullness after the NO-PREFILL WARM filling. Accordingly, the interoceptive awareness measured by online desire to void rating was insignificant. In contrast, in the NO-PREFILL COLD condition, the visceral afferent signals ascended to the posterior insula in IC 26 then further to the anterior insula in IC 16 (the second-order region) resulting in subjective awareness of visceral sensation implied by enhanced desire to void ratings. The information about the interoceptive state also projects to the ACC [2, 15, 17, 146]. Although it is plausible to consider co-activation of the ACC in ICs 26 and 16 for conflict monitoring and focusing attention [154, 155], in the context of our paradigm ACC activity is more consistent with the involvement of the ACC in arousal and initiating autonomic responses related to motivation and goal-directed behaviors [2, 24]. The ACC forms part of the limbic system and has also been shown to play a role in generating an affective response to a stimulus. In addition, the ACC has connections with the motor cortex thus can be involved in selecting appropriate behavioral responses to a stimulus [156]. In previous UB studies, the ACC was implicated in the micturition control including pelvic floor contractions [54, 58, 64, 66, 68], and the PFC was considered to be responsible for planning complex social behaviors, such as whether or not micturition should take place [26]. Taken together, the posterior insular activation in IC 26 indicates unconscious monitoring of afferent signals from the viscera, while upregulation of the anterior insula in IC 16 signifies interoceptive awareness of the visceral sensation with autonomic arousal. Such awareness affords detection of changes in viscera when significant deviations from the homeostatic norm occur and accompanies an incentive motivation (urge/desire) to initiate an action (e.g., voiding) to preserve the body.

Furthermore, changes in the viscera tend to draw attention involuntarily (i.e., bottom-up) as the majority of interoceptive, visceral signals are subliminal. This explains activation of IC 27 covering the bilateral TPJ in the NOPREFILL conditions as TPJ often shows up-regulation during stimulus-triggered bottom-up attentional orientation [157-159]. Previous neuroimaging studies showed that TPJ is

activated in respond to salient stimuli regardless of sensory modality [160, 161]. Furthermore, stimulus-triggered activations in the TPJ usually occur in tandem with the insula [158], which was also observed in our study. Although the conventional temporal-parietal component is right-lateralized, our ICA revealed a bilateral temporal-parietal activation with slightly more pronounced activation on the left. Recent studies indicate that the left temporal-parietal activation may well accompany the right temporal-parietal during stimulus-driven attention [157]. It is also suggested that left-lateralization of the temporal-parietal network may be due to contextual relevance of sensory stimuli [162]. Similarly, the fronto-parietal cortical networks (ICs 30 and 31) are implicated in processing the salient stimuli to facilitate efficient performance of tasks on hand [127]. More specifically, the dorsolateral PFC in ICs 30 and 31 is considered to be responsible for cognitive functions such as evaluation and attention [163, 164] involved in working memory and complex attention tasks [164] as well as anticipation of and attention to visceral sensations and pain [165, 166]. The fact that the left fronto-parietal component (IC 30) was more active than the right fronto-parietal component (IC 31) in our experiment is intriguing but consistent with left-lateralized activation of the dorsolateral PFC observed during the visceral esophageal sensation indicating possible functional differences between the left and right dorsolateral PFC [165, 167].

Table 5 Temporal sorting for I (infusion), F (filled), RF (rating after filled) and D (drainage) trials of the LOW-PREFILL WARM condition

	β-weights: Mean ± SD						One-sample *t*-test: *P*-value[a]					
IC	I	F	RF	D	E	RE	I	F	RF	D	E	RE
IC 11	0.12±0.15	0.08±0.30	0.06±0.29	0.12±0.11	0.13±0.14	0.09±0.25	0.014[b]	0.361	0.446	0.002[b]	0.007[b]	0.238
IC 2	0.08±0.14	0.20±0.26	–0.38±0.20	–0.02±0.20	0.17±0.26	–0.25±0.30	0.068	0.015[b]	0.000[b]	0.683	0.034[b]	0.013[b]
IC 3	0.05±0.09	0.17±0.20	0.06±0.22	0.05±0.16	0.15±0.18	0.01±0.14	0.057	0.009[b]	0.345	0.297	0.013[b]	0.722
IC 33	0.15±0.38	0.10±0.53	–1.28±0.45	0.25±0.20	0.18±0.56	–1.24±0.27	0.170	0.489	0.000[b]	0.001[b]	0.279	0.000[b]

[a]One-sample *t*-test was performed to determine whether the β-weights are statistically different from zero. All *P*-values were uncorrected because these β-weights were not independent between trials for the same IC or between ICs for the same trial.
[b]$P < 0.05$.

Table 6 Temporal sorting for I (infusion), F (filled), RF (rating after filled) and D (drainage) trials of the HIGH-PREFILL WARM condition

	β-weights: Mean ± SD						One-sample *t*-test: *P*-value[a]					
IC	I	F	RF	D	E	RE	I	F	RF	D	E	RE
IC 11	0.19±0.25	0.21±0.24	0.13±0.33	0.14±0.15	0.11±0.18	0.10±0.18	0.019[b]	0.008[b]	0.182	0.005[b]	0.057	0.285
IC 2	0.09±0.16	0.17±0.31	–0.24±0.29	–0.01±0.21	0.22±0.26	–0.13±0.28	0.056	0.063	0.013[b]	0.873	0.010[b]	0.117
IC 3	0.12±0.09	0.19±0.15	0.03±0.16	0.06±0.12	0.15±0.13	0.06±0.16	0.000[b]	0.001[b]	0.514	0.086	0.002[b]	0.216
IC 33	0.20±0.41	0.15±0.54	–1.06±0.39	0.29±0.30	0.21±0.46	–1.28±0.41	0.104	0.326	0.000[b]	0.005[b]	0.131	0.000[b]
IC 9	0.08±0.14	0.05±0.16	0.09±0.21	0.14±0.17	0.04±0.17	0.08±0.17	0.052	0.304	0.124	0.018[b]	0.403	0.110
IC 12	0.12±0.19	0.08±0.41	0.10±0.25	0.05±0.24	–0.04±0.32	0.00±0.21	0.045[b]	0.482	0.165	0.497	0.682	0.936
IC 24	0.00±0.18	0.18±0.25	0.89±0.30	0.03±0.20	0.03±0.28	0.66±0.32	0.966	0.024[b]	0.000[b]	0.629	0.683	0.000[b]

[a]One-sample *t*-test was performed to determine whether the β-weights are statistically different from zero. All *P*-values were uncorrected because these β-weights were not independent between trials for the same IC or between ICs for the same trial.
[b]$P < 0.05$.

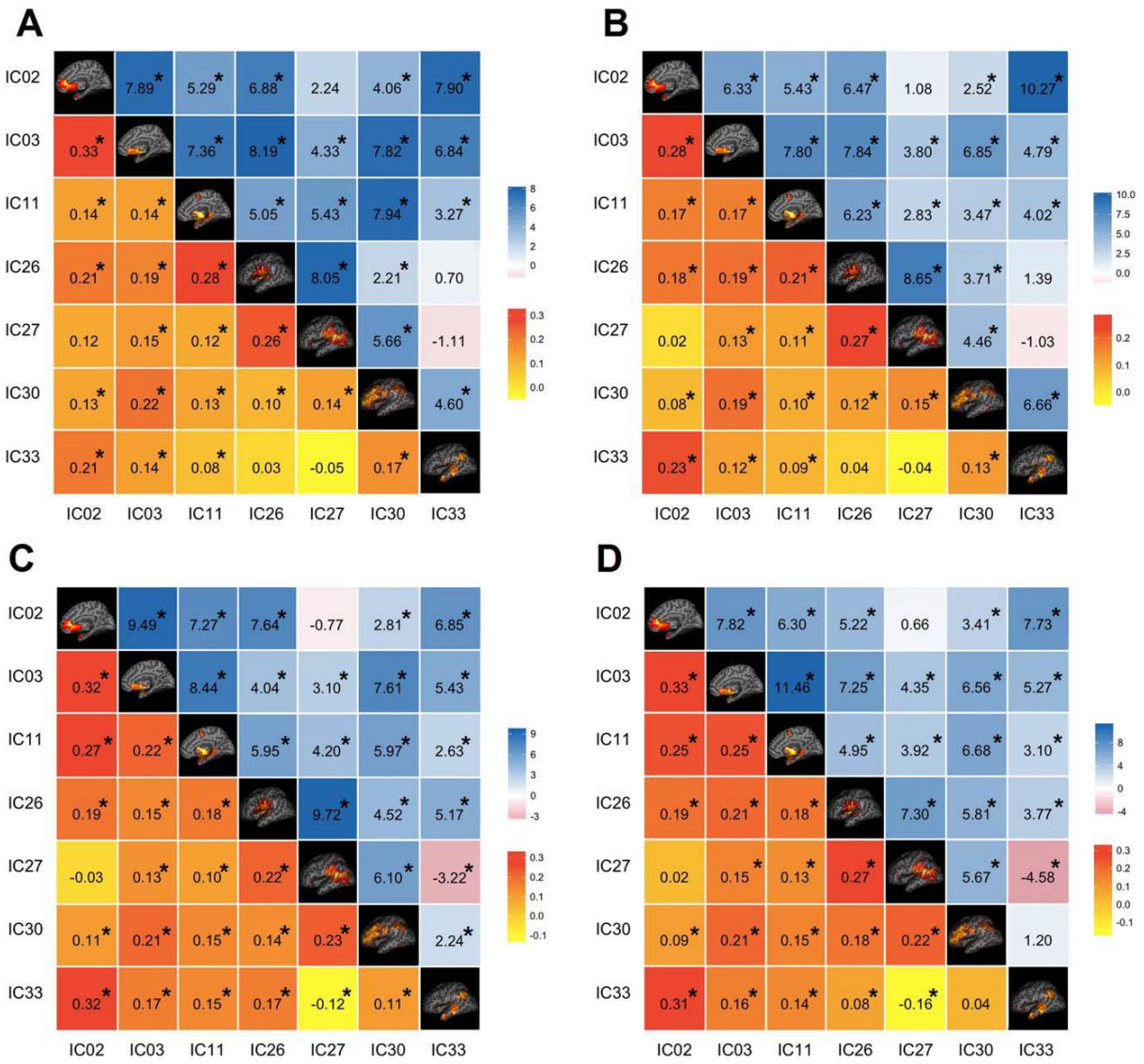

Figure 7 Functional Network Connectivity (FNC) between the task-related networks. (A) The NO-PREFILL WARM condition; (B) The NO-PREFILL COLD condition; (C) The LOW-PREFILL WARM condition; (D) The HIGH-PREFILL WARM condition. The lower half of matrix is the mean of FNC correlation pairs, the upper half is the *t*-value of each correlation pair resulted from Student's *t*-test. The black asterisk indicates the pairs surviving the *t*-test with an FDR-corrected *P*-value of 0.05.

The transient relay of visceral afferents in thalamus on their way to the insula was also captured by significant activation of the IC 24 during the COLD filling. Activation of the posterior insula during "drainage" phase in both NO-PREFILL WARM and COLD conditions implies the afferent fiber response to the UB emptying and consequent (re-)mapping of current visceral state. In the NO-PREFILL WARM, ICs 35 and 22 also showed up-regulation during "drainage." The activity of IC 35, which involves the default-mode network, can be related to previous findings that show stimulus-induced activity during tasks with low cognitive load [41, 168]. Alternatively, IC 35 may be recruited for introspective interrogation such as autobiographical memory, and self-monitoring [169, 170]. Upregulation of IC 22 during NO-PREFILL WARM drainage can be interpreted as activation of the IFG and limbic association areas including the bilateral hippocampi and parahippocampal gyri as well as the thalamus, midbrain and brainstem. Previous studies showed such network of brain regions in

particular involving the limbic association areas is strongly associated with interoceptive processing elicited during air-hunger, olfactory and gustatory responses [124]. The midbrain/brainstem activation observed as part of this component can be related to the midbrain PAG (the mesencephalic homeostatic motor center), which relays information to the pons in brainstem and back to the sacral parasympathetic nerves during the UB emptying [59, 63, 171]. This is also consistent with previous neuroimaging studies of the UB stimulation where activation of the right IFG [52, 54, 58, 63], thalamus [53, 55-57, 66], PAG [52, 53, 55-57, 59, 63, 64, 66], and pons [52, 53, 59, 63, 64, 66] were observed.

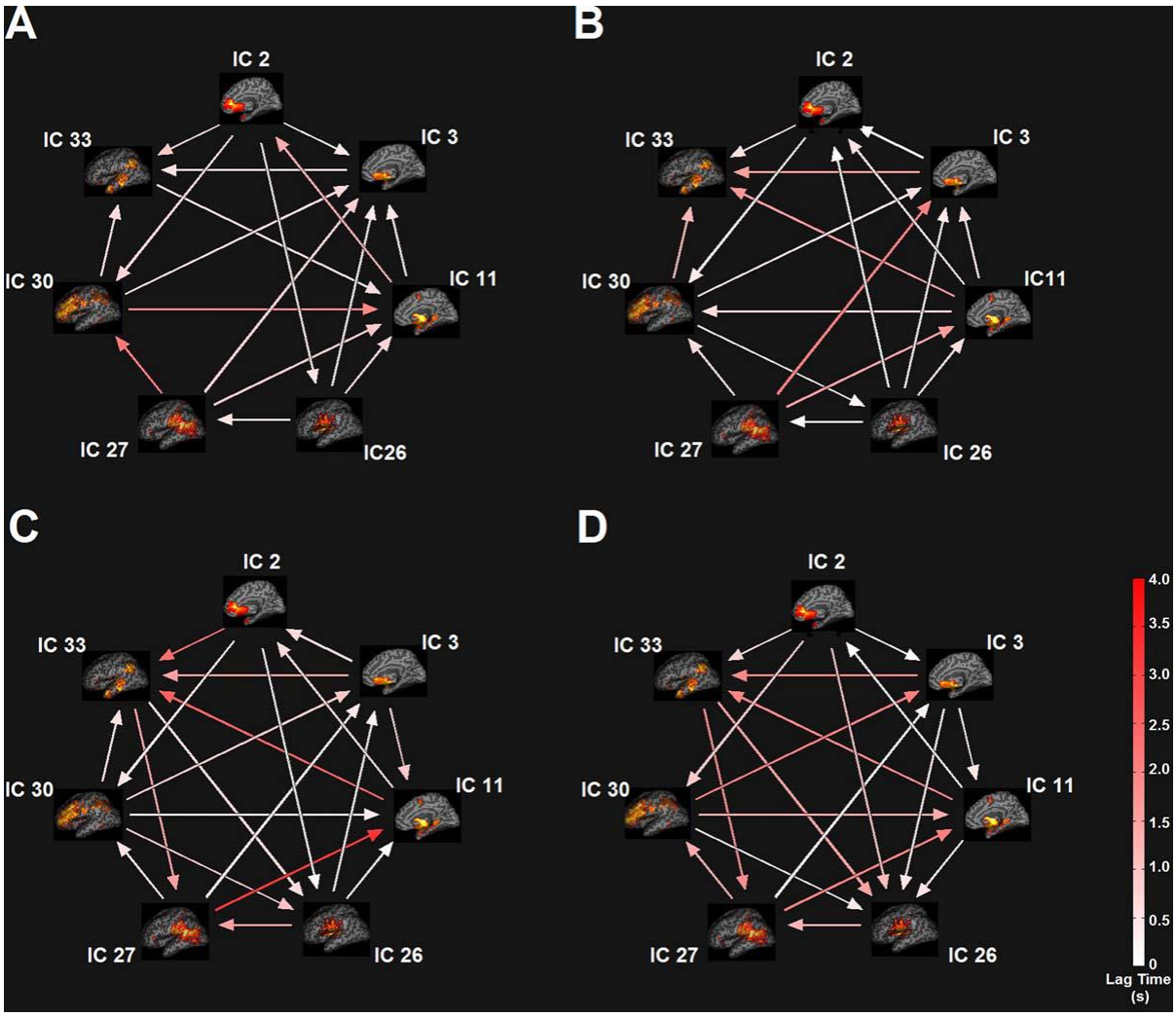

Figure 8 Functional Network Connectivity (FNC) between the task-related networks. (A) The NO-PREFILL WARM condition; (B) The NO-PREFILL COLD condition; (C) The LOW-PREFILL WARM condition; (D) The HIGH-PREFILL WARM condition. Arrow represents a significant correlation between a network pair ($P < 0.05$, FDR-corrected). The direction of the arrows indicates the time lag between the pairs. Color bar shows lag in seconds.

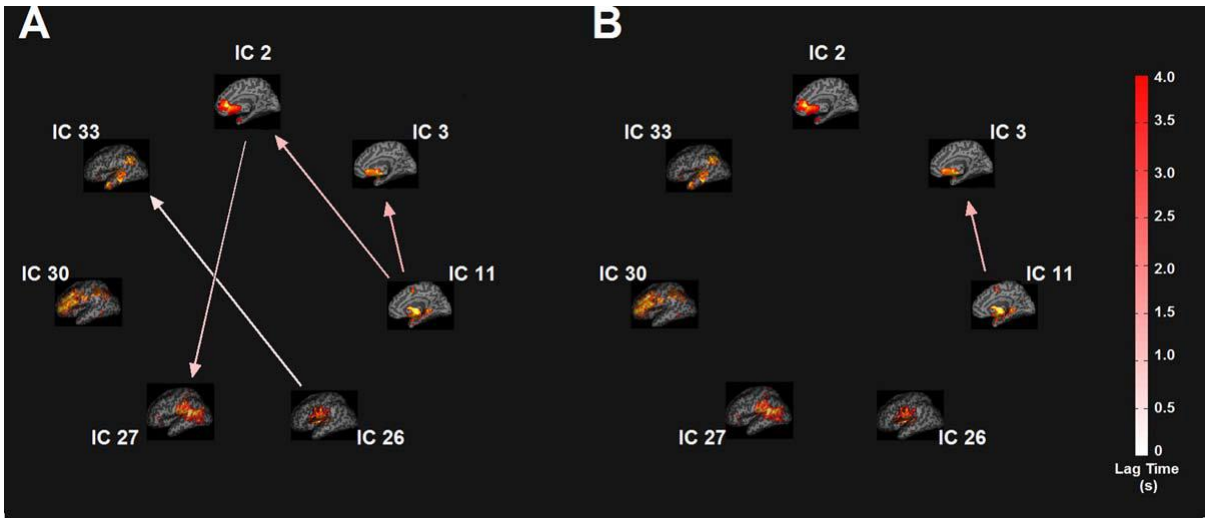

Figure 9 FNC difference between task-related network pairs between task conditions. (A) The NO-PREFILL WARM and the LOWPREFILL WARM condition pairs; (B) The NO-PREFILL WARM and the HIGH-PREFILL WARM condition pairs. Arrow represents a significant correlation between a network pair ($P < 0.05$, FDR-corrected). The direction of the arrows indicates the time lag between the pairs. Color bar shows lag in seconds.

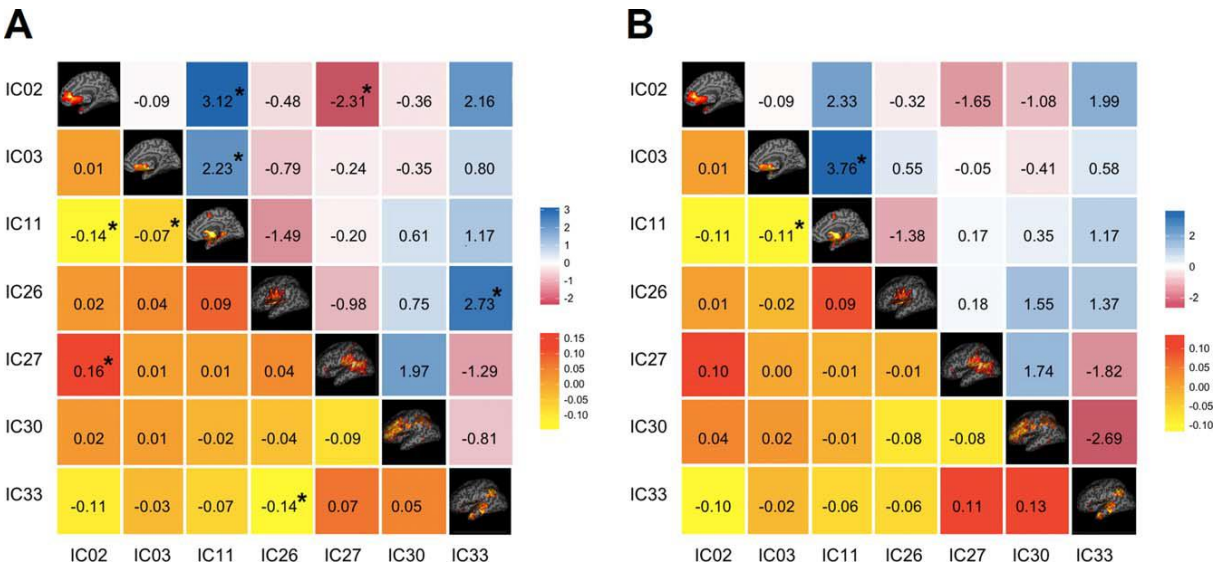

Figure 10 FNC difference between task-related network pairs between task conditions. (A) The NO-PREFILL WARM and the LOWPREFILL WARM condition pairs; (B) The NO-PREFILL WARM and the HIGH-PREFILL WARM condition pairs. The lower half of matrix is the mean correlation difference between network pairs between two tasks. The upper half is the *t*-value resulting from paired *t*-test with FDR corrected *P*-value of 0.05. The black asterisk indicates the pairs surviving the *t*-test with an FDR-corrected *P*-value.

NETWORK MODULATION DURING DISTENTION PRESSURE ON THE VISCERA

During the LOW- and HIGH-PREFILL WARM conditions, ICs 2, 3, 11, and 33 showed activity increases. In addition to the said components, during the HIGHPREFILL WARM condition, modulation of ICs 9, 12, and 24 were also observed. At the LOW- to HIGH-PREFILL relative to NO-PREFILL WARM condition, participants were already aware of their UB fullness, thus eradicating a need for bottom-up deployment of attentional resources (i.e., no activation of IC 27 involving TPJ). Instead, the

task condition imposed modulations of component involved in top-down control of the visceral sensation (e.g., withholding of the urine) as well as the viscerosensory alliesthesia. Alliesthesia (from allios, changed, and esthesia, sensation) refers to the modulation of hedonic aspects of a stimulus by the homeostatic (internal) state of the body [172]. In the case of the UB, the viscerosensory alliesthesia is the feeling of unpleasantness a subject experiences as distention pressure on the viscera increases. This affective appraisal of viscerosensory alliesthesia recruits IC 2 involving the ventral ACC and the adjacent ventromedial PFC and IFG, IC 3 comprising bilateral amygdala, parahippocampal gyri and midbrain, and IC 11 with bilateral striatum, insula, and thalamus. Elevated activation in limbic regions, including the striatum, amygdala, ACC and medial PFC can be also associated with increased unpleasantness with increased desire to void in response to increased distention pressure on the viscera. Cognitive inhibition, however, can postpone voiding despite increased urge.

The PFC is defined as that part of the frontal lobe that lies anteriorly to the premotor areas (BA 9, 10, 46) that are involved in the planning of complex motor actions, and the primary motor regions, which mediate conscious movement. Anatomically, the ventral PFC can be divided into orbital and medial sections. The more lateral parts of the PFC are involved in aspects of cognition, especially working memory [173], while the ventromedial regions seem to be involved in decision-making especially in an emotional and social context [174]. The role of the frontal lobes in control of micturition has been previously investigated (for a review of the micturition switch and its forebrain influences see [175]). In our earlier study in healthy subjects performing pelvic floor contractions with empty and full UB, we showed that medial PFC activity is involved in the control of micturition, while limbic system was likely involved in inhibition of the voiding control mechanism [67]. In animal lesion as well as neuroimaging studies, forebrain structures including the PFC and the ACC were found to play a modulatory role in the firing of the voiding reflex [52, 55, 59, 63, 176, 177]. Similar observations have been reported in patients with spinal cord lesions [78], PFC underperfusion [178], and stroke [179]. In fact, the significance of the PFC in the continence and healthy UB function was initially established in clinical studies by Ueki [201], and Andrew and Nathan [176]. The latter researchers showed that lesions in the white matter tracts located in the medial PFC caused lasting urinary tract dysfunction while lesions in the gray-matters in medial PFC led to transient dysfunction (relatively short-term incontinence) [25, 180]. These data indicate that the medial PFC has a pivotal role in the top-down control of the visceral sensation although the foci of PFC activation are not consistent among studies.

Furthermore, meta-analysis of neuroimaging studies implies involvement of brain regions encompassed in IC 2 (in particular the ventromedial PFC) in the top-down modulation between sensory, self-referential, and higher-order processing [181]. Neuroanatomical studies have revealed reciprocal connections not only between the ventromedial PFC and PAG, which mediate the visceral autonomic activity, but also between the ventromedial PFC and limbic regions, including the ventral striatum and amygdala [7]. During the storage and micturition phases, IFG, part of the PFC, has been seen to be active [52, 54, 58, 63], as well as the orbitofrontal cortex [58]. Previous studies showed activation in the orbitofrontal cortex is related to affective decision-making, and reward valuation in hedonic experiences [182]. Dopamine is crucially involved in reward valuation as well as the reinforcement learning and habit development [183, 184]. The brain's reward system synthesizes both

the bottom-up and top-down inputs from the ventral striatum (IC 11), the ventromedial PFC and the ACC (IC 2) to create an integrated view of the subjective value of a stimulus. As such, IC 2 activation observed in our study may reflect not only the cortical control of the visceral autonomic system (via hypothalamus and the PAG), but more importantly the affective appraisal of increased visceral pressure (via striatum, IC 11, and amygdala, IC 3). An intermediate step in this operation is the production of "somatic markers," which signals the intensity (salience) of the valence (negative value) of the stimulus (visceral pressure) experienced by subjects [5]. Together with ICs 2 and 11, this "fronto-insula-limbic-striatal" system helps to identify the emotional salience of interoceptive stimuli, regulate the viscera-affective state, and motivate action to retain psychophysical homeostasis. Activation of this system in our study is in line with the James–Lange theory of emotion [185, 186] which underlies the role of physiologic and cognitive responses in the formation of emotion [174, 187]. Critical to our survival as a species is the acquisition of the social cognition, a complex phenomenon that entails awareness of one's self as well as the perception of others [i.e., linking "I do and I feel" with "she does and she feels" [188]]. For example, loss of the UB control and thus voiding or leakage is socially undesirable and highly embarrassing for both the sufferer and those who witness it; thus planning and assessment of the appropriateness of when to void are deeply linked not only to our ability to sense and perceive the physiological condition of our body, but also to the social appropriateness of action [175]. Such unique human faculty (i.e., social cognition) is instantiated in the medial PFC [189].

The absence of direct activation in the posterior insula in IC 26, and the anterior insula in IC 16, key areas in salience detection was perhaps surprising. However, absence of insular activation during the UB stimulation has also been noted in other studies with high-level artificial UB filling [65, 190]. The insula is most activated during changing salience (such as rapid change in distention pressure) and its activity is reported in the "early" evaluation of the significance of sensory and affective stimuli presented [191]. However, in the LOW- and HIGH-PREFILL WARM conditions compared to the NO-PREFILL condition, the prefilled UB levels might have prevented detection of significant changes in salience. We also find Komesu et al. [65] argument for the lack of insular activation due to habituation caused by repetitive stimulation of the UB plausible. IC 11 showed activity increases during almost all phases of LOW- and HIGH-PREFILL WARM tasks. A closer look at ICs 11, 16, and 26 reveals considerable overlap of these components at insula (**Supporting Figure 4**). Note that the spatial ICA algorithm attempts to identify maximally independent sets of spatial maps (which can overlap) each of which are represented by a strongly coherent or correlated time course [192]. Component overlap has been observed in previous ICA studies and has been interpreted as evidence of multiple concurrent central processes associated with common brain regions [193, 194].

In our previous fMRI investigation of the supraspinal central representation of the UB stimulation [58, 69], similar to the current study, one of the most prominent activated brain areas during the UB cooling was the insula but with prominent right-lateralized activation in the right-handed subjects. In this study, we also observed slightly prominent right-sided activity in insula (both ICs 16 and 26) as well as in IC 3. Previous neuroanatomical studies demonstrated that small-diameter sympathetic afferent fibers provide input to lamina I while small-diameter parasympathetic afferents project to the nucleus of the solitary tract in medulla [17]. However, the parasympathetic activity is postulated to be re-represented

in the left (dominant) hemisphere, whereas the sympathetic activity is assumed to be re-represented in the right (non-dominant) hemisphere [17]. The right-lateralization of the insular components that we observed in relation to the visceral stimulation of the UB might be related to the greater activation of the sympathetic afferent fibers compared to their parasympathetic counterparts. Considering the autonomic regulation of the UB, the sympathetic activity causes the internal urethral sphincter to close allowing the UB to fill. At the same time, moderate UB distension inhibits parasympathetic activity, which would otherwise contract the UB to start the voiding process [195]. Therefore, during visceral (thermal and mechanical) stimulation of the UB, the sympathetic activity seems to outweigh the parasympathetic activity in order to allow urine accumulation (UB muscle relaxation), and prevent voiding (and UB contraction). These re-representations of both sympathetic and parasympathetic afferents are postulated to provide the foundation for a subjective evaluation of interoceptive state, which is forwarded to the PFC especially the ventromedial and orbitofrontal cortices where hedonic valence is represented [17]. The lateralization of the component activations can also be related to the hemispheric dominance in the supraspinal processing of the UB sensations. Such hemispheric asymmetry has been previously reported not only for UB sensations [58, 64, 69] but also other visceral functions such as the ano-rectal motor function [196]. The significance of the lateralized cortical representations of visceral sensations is still unknown.

The HIGH-PREFILL WARM paradigm in our study also revealed significant cerebellar activation, namely in ICs 9 and 12. Previous studies showed cerebellar activation following increasing UB filling [57, 60, 63]. Furthermore, cerebellar lesions can disrupt both storage and expulsion [197]. Thus, the cerebellum seems to be involved in processing sensory information of UB filling and motor control of micturition.

FUNCTIONAL NETWORK CONNECTIVITY DURING VISCERAL INTEROCEPTION

We performed FNC using maximal correlation on back-reconstructed subject-specific time courses of seven task-modulated networks. FNC, a measure of inter-network connectivity, is weaker than intranetwork connectivity [108]. The average ± standard deviation of FNC values were 0.154 ± 0.111, 0.141 ± 0.103, 0.161 ± 0.120, and 0.161 ± 0.112 for the NO-PREFILL WARM, NO-PREFILL COLD, LOW-PREFILL WARM, and HIGH-PREFILL WARM conditions, respectively. As shown in **Figure 7**, most of the correlations are positive. Across different conditions, the FNC correlation between networks was the weakest between IC 33 involving posterior parts of the default mode network, namely the posterior midline structures of the precuneus/posterior cingulate cortex and the bilateral inferior parietal lobules [139, 140] and IC 27 centered on the bilateral TPJ. The correlations value for this network pair was negative at all times, i.e., –0.05, –0.04, –0.12 and –0.16 for the NO-PREFILL WARM, NOPREFILL COLD, LOW-PREFILL WARM, and HIGHPREFILL WARM conditions, respectively. The anticorrelation between the TPJ in IC 27 and the regions comprising the posterior midline structures in IC 33 is consistent with previous finding [198]. Across all conditions, the strongest FNC correlation was always between IC 2 encompassing the ventromedial PFC, and IC 3 involving

the bilateral amygdala, and parahippocampal gyri, i.e., 0.33, 0.28, 0.32, and 0.33 for the NO-PREFILL WARM, NOPREFILL COLD, LOW-PREFILL WARM, and HIGHPREFILL WARM conditions, respectively.

The present FNC demonstrated that the connectivity of IC 33 covering the more posterior default mode component with other ICA components significantly ($P < 0.05$, FDR-corrected) differed during the visceral stimulation. In the NO-PREFILL conditions, there was no FNC between IC 33 and IC 26 involving the posterior insula, or between IC 33 and IC 27 focused at the TPJ. In the HIGH-PREFILL WARM, the FNC between ICs 33 and IC 30, the left fronto-parietal network, was also not significant. Much of the regions in ICs 26, 30, and 27 that showed nonsignificant FNC with IC 33, overlap with the so-called task-positive network including the dorsolateral and ventral PFC, insula, and attention networks [41]. Uddin et al. [170] also showed that posterior midline structures of the precuneus/posterior cingulate cortex has an antagonistic relationship with prefrontal-based motor planning and control circuits. In addition to the above network pairs, the FNC between ICs 2 and 27 was not significant for all conditions ($P < 0.05$, FDR-corrected). The main node in IC 2 is the ventromedial PFC, which resembles the anterior node of the default mode network. The main node of IC 27 is the TPJ (more left-lateralized here) which is suggested to be involved in integrating contextual knowledge with incoming sensory information through interactions with the insula and the frontopariental networks [162]. Kucyi et al. [198] showed previously that both the right and left TPJ exhibit negative functional connectivity with the default mode network (e.g., medial PFC, precuneus/posterior cingulate cortex). Consequently, the lack of FNC between ICs 2 and 27 can also be interpreted as the lack of correlation between the task-positive and task-negative networks.

An intriguing finding of our study is that compared to the NO-PREFILL WARM condition, both LOW- and HIGH-PREFILL WARM conditions showed significantly increased FNC between ICs 11 and 3 ($P < 0.05$, FDR-corrected); i.e., 0.14 ± 0.07 for the NO-PREFILL WARM condition compared to 0.22 ± 0.09, 0.25 ± 0.08 for the LOW- and HIGH-PREFILL WARM conditions, respectively. The enhanced FNC between these two ICA components in the LOW- and HIGH-PREFILL WARM conditions may represent an increased crosstalk between these two networks once the awareness of the visceral stimulation is achieved. Moreover, FNC comparison between the NO-PREFILL WARM and LOW-PREFILL WARM conditions revealed there are significant difference in FNC between (i) ICs 2 and 27, (ii) ICs 2 and 11, and (iii) ICs 33 and 26 ($P < 0.05$, FDR-corrected). A major behavioral distinction between the NO-PREIFLL WARM and LOW-PREFILLE WARM is a shift from non-conscious visceral sensation to conscious feeling (interoceptive awareness). As discussed earlier, this shift in awareness activates the fronto-insula-limbic-striatal system, which starts a cascade of events including regulation of the autonomic and arousal states as well as motivating action in response to increased viscerosensory alliesthesia with the aim of retaining homeostasis. This reallocation of activity from the salience detection circuitry to affective-arousal-motivation networks with the onset of subjective conscious experience echoes well with a largescale reorganization of FNC in which the FNC between ICs 2 and 27 significantly decreased (i.e., from 0.12 ± 0.17 to -0.03 ± 0.15, $P < 0.05$, FDR-corrected), while the FNC between ICs 2 and 11 were significantly increased (i.e., from 0.14 ± 0.09 to 0.27 ± 0.12, $P < 0.05$, FDR-corrected). The significant increase between ICs 33 and 26 (i.e., from 0.03 ± 0.14 to 0.17 ± 0.11, $P < 0.05$, FDR-corrected) can also be related to increased crosstalk between the primary

interoceptive cortex involved in representing bodily state and the autobiographical activity of the default mode network.

CAVEATS AND FUTURE DIRECTION

There are some important caveats that must be considered in the interpretation of our results. First, we included only female subjects to control for the confounding factor of sex-related differences in visceral interoception, and better ability to perform non-painful catheterization. Second, the long acquisition time of the datasets (15–17 min per task condition) has benefited the precision of estimation of FNC correlations. Conversely, longer fMRI time series are more prone to subjects' distraction, thus less likely to represent a stable brain functional state. Third, although our analysis was based on adequate sampling of imaging data from each subject, there was a modest number of subjects in the final sample. Thus, the findings certainly deserve replication with a larger sample size of both genders using more time-optimized viscerosensory paradigm. Another potential limitation is the possible contamination of the BOLD signals related to the visceral stimulation with the brain activates related to the rating. Although we explicitly instructed the subjects not to mentally perform the subjective estimation of the rating during the event periods prior to the motor task of moving the manipulandum on the response box (and none of the subjects reported doing so in the post-scan questionnaires), it is difficult to be sure when subjects start to think about what. On the other hand, this thinking process cannot be completely excluded; after all this is probably an integral part of interoceptive feeling. There is also a possibility of false negatives due to thresholding and smearing of activity from individual participants. Lastly, our experiment was performed with the UB as a representative internal organ, in which the translation of the UB volume and fluid temperature into sensory afferent activity lies at the heart of the interoceptive process. Despite this constraint, we believe our observations can potentially be compared to interoception from other visceral organs such as GI tract as neuroimaging studies of especially lower GI tract showed activations in similar brain areas to the UB [25, 27, 71, 72]. However, as a strong point of this study, we emphasize that we used ICA as a model free model with no bias in selecting the activation regions. To add to fidelity of our results, we particularly followed the ICA procedure that is suggested to yield more robust and reliable components in the literature (e.g., the GICA-3 back-reconstruction algorithm [113], intensity normalization in preprocessing [99], 100 runs with random initiation in ICASSO [112]).

In conclusion, ICA and FNC analysis revealed that visceral interoception is a dynamic process that involves closely interacting, yet dissociable components. Within this system, the posterior and anterior insula, ACC, dorsolateral PFC and posterior parietal cortex, thalamus, and TPJ provide monitoring of visceral state and salience detection, whereas the ventromedial PFC, IFG, ventral striatum, insula, ACC, amygdala, parahippocampal gyri, midbrain are more likely to be involved in the regulation of the arousal, motivational and affective states and action initiation. Future studies are expected to further detail the role of these intrinsic networks in interoception and its effect on human conscious experience, and emotional states.

ACKNOWLEDGMENT

This study was supported by the Swiss National Science Foundation (grant number: 135774).

REFERENCES

1. Cameron OG. Interoception: the inside story--a model for psychosomatic processes. Psychosom Med. 2001;63(5):697-710.
2. Craig AD. Interoception: the sense of the physiological condition of the body. Curr Opin Neurobiol. 2003;13(4):500-5.
3. Craig AD. Interoception and emotion: A neuroanatomical perspective. In: Lewis M, Haviland-Jones JM, Feldman Barrett L, editors. Handbook of Emotions. New York: Guilford Press. 2008:2722-88.
4. Critchley HD. Neural mechanisms of autonomic, affective, and cognitive integration. J Comp Neurol. 2005;493(1):154-66.
5. Damasio AR. The Feeling of What Happens: Body, Emotion and the Making of Consciousness. New York: Harcourt Brace & Company. 2000.
6. Denton DA, McKinley MJ, Farrell M, Egan GF. The role of primordial emotions in the evolutionary origin of consciousness. Conscious Cogn. 2009;18(2):500-14.
7. Saper CB. The central autonomic nervous system: conscious visceral perception and autonomic pattern generation. Annu Rev Neurosci. 2002;25:433-69.
8. Habler HJ, Janig W, Koltzenburg M. Myelinated primary afferents of the sacral spinal cord responding to slow filling and distension of the cat urinary bladder. J Physiol. 1993;463:449-60.
9. Janig W, Morrison JF. Functional properties of spinal visceral afferents supplying abdominal and pelvic organs, with special emphasis on visceral nociception. Prog Brain Res. 1986;67:87-114.
10. Kanai A, Andersson KE. Bladder afferent signaling: recent findings. J Urol. 2010;183(4):1288-95.
11. Fall M, Lindstrom S, Mazieres L. A bladder-to-bladder cooling reflex in the cat. J Physiol. 1990;427:281-300.
12. Habler HJ, Janig W, Koltzenburg M. Activation of unmyelinated afferent fibres by mechanical stimuli and inflammation of the urinary bladder in the cat. J Physiol. 1990;425:545-62.
13. Craig AD. A new view of pain as a homeostatic emotion. Trends Neurosci. 2003;26(6):303-7.
14. Blomqvist A, Zhang ET, Craig AD. Cytoarchitectonic and immunohistochemical characterization of a specific pain and temperature relay, the posterior portion of the ventral medial nucleus, in the human thalamus. Brain. 2000;123 Pt 3:601-19.
15. Craig AD, Bushnell MC, Zhang ET, Blomqvist A. A thalamic nucleus specific for pain and temperature sensation. Nature. 1994;372(6508):770-3.
16. Craig AD. Topographically organized projection to posterior insular cortex from the posterior portion of the ventral medial nucleus in the long-tailed macaque monkey. J Comp Neurol. 2014;522(1):36-63.
17. Craig AD. How do you feel? Interoception: the sense of the physiological condition of the body. Nat Rev Neurosci. 2002;3(8):655-66.
18. Evrard HC, Logothetis NK, Craig AD. Modular architectonic organization of the insula in the macaque monkey. J Comp Neurol. 2014;522(1):64-97.

19. Kurth F, Zilles K, Fox PT, Laird AR, Eickhoff SB. A link between the systems: functional differentiation and integration within the human insula revealed by meta-analysis. Brain Struct Funct. 2010;214(5-6):519-34.

20. Wager TD, Barrett LF. From affect to control: Functional specialization of the insula in motivation and regulation. Published online at PsycExtra. 2004.

21. Brooks JC, Zambreanu L, Godinez A, Craig AD, Tracey I. Somatotopic organisation of the human insula to painful heat studied with high resolution functional imaging. Neuroimage. 2005;27(1):201-9.

22. Cameron OG, Minoshima S. Regional brain activation due to pharmacologically induced adrenergic interoceptive stimulation in humans. Psychosom Med. 2002;64(6):851-61.

23. Critchley HD, Corfield DR, Chandler MP, Mathias CJ, Dolan RJ. Cerebral correlates of autonomic cardiovascular arousal: a functional neuroimaging investigation in humans. J Physiol. 2000;523 Pt 1:259-70.

24. Critchley HD, Mathias CJ, Josephs O, O'Doherty J, Zanini S, Dewar BK, et al. Human cingulate cortex and autonomic control: converging neuroimaging and clinical evidence. Brain. 2003;126(Pt 10):2139-52.

25. Fowler CJ, Griffiths DJ. A decade of functional brain imaging applied to bladder control. Neurourol Urodyn. 2010;29(1):49-55.

26. Kavia RB, Dasgupta R, Fowler CJ. Functional imaging and the central control of the bladder. J Comp Neurol. 2005;493(1):27-32.

27. Mayer EA. Gut feelings: the emerging biology of gut-brain communication. Nature Reviews Neuroscience. 2011;12(8):453-66.

28. Lerner A, Bagic A, Hanakawa T, Boudreau EA, Pagan F, Mari Z, et al. Involvement of insula and cingulate cortices in control and suppression of natural urges. Cereb Cortex. 2009;19(1):218-23.

29. Craig AD, Chen K, Bandy D, Reiman EM. Thermosensory activation of insular cortex. Nat Neurosci. 2000;3(2):184-90.

30. Liotti M, Brannan S, Egan G, Shade R, Madden L, Abplanalp B, et al. Brain responses associated with consciousness of breathlessness (air hunger). P Natl Acad Sci USA. 2001;98(4):2035-40.

31. Denton D, Shade R, Zamarippa F, Egan G, Blair-West J, McKinley M, et al. Neuroimaging of genesis and satiation of thirst and an interoceptor-driven theory of origins of primary consciousness. Proc Natl Acad Sci U S A. 1999;96(9):5304-9.

32. Egan G, Silk T, Zamarripa F, Williams J, Federico P, Cunnington R, et al. Neural correlates of the emergence of consciousness of thirst. Proc Natl Acad Sci U S A. 2003;100(25):15241-6.

33. Teves D, Videen TO, Cryer PE, Powers WJ. Activation of human medial prefrontal cortex during autonomic responses to hypoglycemia. Proc Natl Acad Sci U S A. 2004;101(16):6217-21.

34. Naqvi NH, Bechara A. The hidden island of addiction: the insula. Trends Neurosci. 2009;32(1):56-67.

35. Beckmann CF, Smith SM. Probabilistic independent component analysis for functional magnetic resonance imaging. IEEE Trans Med Imaging. 2004;23(2):137-52.

36. Calhoun VD, Adali T, Pearlson GD, van Zijl PC, Pekar JJ. Independent component analysis of fMRI data in the complex domain. Magn Reson Med. 2002;48(1):180-92.

37. McKeown MJ, Makeig S, Brown GG, Jung TP, Kindermann SS, Bell AJ, et al. Analysis of fMRI data by blind separation into independent spatial components. Human Brain Mapping. 1998;6(3):160-88.

38. Norman KA, Polyn SM, Detre GJ, Haxby JV. Beyond mind-reading: multi-voxel pattern analysis of fMRI data. Trends Cogn Sci. 2006;10(9):424-30.

39. Friston K. Beyond phrenology: What can neuroimaging tell us about distributed circuitry. An Rev Neurosci. 2002;25:221-50.

40. Cordes D, Haughton V, Carew JD, Arfanakis K, Maravilla K. Hierarchical clustering to measure connectivity in fMRI resting-state data. Magn Reson Imaging. 2002;20(4):305-17.

41. Fox MD, Snyder AZ, Vincent JL, Corbetta M, Van Essen DC, Raichle ME. The human brain is intrinsically organized into dynamic, anticorrelated functional networks. Proc Natl Acad Sci U S A. 2005;102(27):9673-8.

42. Calhoun VD, Adali T, Pearlson GD, Pekar JJ. A method for making group inferences from functional MRI data using independent component analysis. Hum Brain Mapp. 2001;14(3):140-51.

43. Jafri MJ, Pearlson GD, Stevens M, Calhoun VD. A method for functional network connectivity among spatially independent resting-state components in schizophrenia. Neuroimage. 2008;39(4):1666-81.

44. Erhardt EB, Allen EA, Damaraju E, Calhoun VD. On network derivation, classification, and visualization: a response to Habeck and Moeller. Brain Connect. 2011;1(2):1-19.

45. Calhoun VD, Kiehl KA, Pearlson GD. Modulation of temporally coherent brain networks estimated using ICA at rest and during cognitive tasks. Hum Brain Mapp. 2008;29(7):828-38.

46. Smith SM, Fox PT, Miller KL, Glahn DC, Fox PM, Mackay CE, et al. Correspondence of the brain's functional architecture during activation and rest. Proc Natl Acad Sci U S A. 2009;106(31):13040-5.

47. Damasio AR. Looking for Spinoza: Joy, sorrow, and the feeling brain. New York, NY: Harvest. 2004.

48. Damasio AR. Descartes' Error: Emotion, Reason and the Human Brain. New York, NY: Random House. 2008.

49. Damasio AR, Grabowski TJ, Bechara A, Damasio H, Ponto LL, Parvizi J, et al. Subcortical and cortical brain activity during the feeling of self-generated emotions. Nat Neurosci. 2000;3(10):1049-56.

50. LeDoux JE. Synaptic Self: How Our Brains Become Who We Are. New York: Viking. 2002.

51. Fowler CJ, Griffiths D, de Groat WC. The neural control of micturition. Nat Rev Neurosci. 2008;9(6):453-66.

52. Blok BF, Sturms LM, Holstege G. Brain activation during micturition in women. Brain. 1998;121 (Pt 11):2033-42.

53. Griffiths D, Derbyshire S, Stenger A, Resnick N. Brain control of normal and overactive bladder. J Urol. 2005;174(5):1862-7.

54. Griffiths D, Tadic SD, Schaefer W, Resnick NM. Cerebral control of the bladder in normal and urge-incontinent women. Neuroimage. 2007;37(1):1-7.

55. Kuhtz-Buschbeck JP, van der Horst C, Pott C, Wolff S, Nabavi A, Jansen O, et al. Cortical representation of the urge to void: a functional magnetic resonance imaging study. J Urol. 2005;174(4 Pt 1):1477-81.

56. Kuhtz-Buschbeck JP, Gilster R, van der Horst C, Hamann M, Wolff S, Jansen O. Control of bladder sensations: an fMRI study of brain activity and effective connectivity. Neuroimage. 2009;47(1):18-27.

57. Matsuura S, Kakizaki H, Mitsui T, Shiga T, Tamaki N, Koyanagi T. Human brain region response to distention or cold stimulation of the bladder: A positron emission tomography study. J Urology. 2002;168(5):2035-9.

58. Mehnert U, Boy S, Svensson J, Michels L, Reitz A, Candia V, et al. Brain activation in response to bladder filling and simultaneous stimulation of the dorsal clitoral nerve - An fMRI study in healthy women. Neuroimage. 2008;41(3):682-9.

59. Michels L, Blok BF, Gregorini F, Kurz M, Schurch B, Kessler TM, et al. Supraspinal Control of Urine Storage and Micturition in Men--An fMRI Study. Cereb Cortex. 2015;25(10):3369-80.

60. Nour S, Svarer C, Kristensen JK, Paulson OB, Law I. Cerebral activation during micturition in normal men. Brain. 2000;123 (Pt 4):781-9.

61. Tadic SD, Griffiths D, Schaefer W, Resnick NM. Abnormal connections in the supraspinal bladder control network in women with urge urinary incontinence. Neuroimage. 2008;39(4):1647-53.

62. Tadic SD, Griffiths D, Schaefer W, Murrin A, Clarkson B, Resnick NM. Brain activity underlying impaired continence control in older women with overactive bladder. Neurourol Urodyn. 2012;31(5):652-8.

63. Athwal BS, Berkley KJ, Hussain I, Brennan A, Craggs M, Sakakibara R, et al. Brain responses to changes in bladder volume and urge to void in healthy men. Brain. 2001;124(Pt 2):369-77.

64. Blok BF, Willemsen AT, Holstege G. A PET study on brain control of micturition in humans. Brain. 1997;120 (Pt 1):111-21.

65. Komesu YM, Ketai LH, Mayer AR, Teshiba TM, Rogers RG. Functional MRI of the Brain in Women with Overactive Bladder: Brain Activation During Urinary Urgency. Female Pelvic Med Reconstr Surg. 2011;17(1):50-4.

66. Seseke S, Baudewig J, Kallenberg K, Ringert RH, Seseke F, Dechent P. Voluntary pelvic floor muscle control--an fMRI study. Neuroimage. 2006;31(4):1399-407.

67. Zhang H, Reitz A, Kollias S, Summers P, Curt A, Schurch B. An fMRI study of the role of suprapontine brain structures in the voluntary voiding control induced by pelvic floor contraction. Neuroimage. 2005;24(1):174-80.

68. Di Gangi Herms AM, Veit R, Reisenauer C, Herms A, Grodd W, Enck P, et al. Functional imaging of stress urinary incontinence. Neuroimage. 2006;29(1):267-75.

69. Mehnert U, Michels L, Zempleni MZ, Schurch B, Kollias S. The Supraspinal Neural Correlate of Bladder Cold Sensation-An fMRI Study. Human Brain Mapping. 2011;32(6):835-45.

70. Mayer EA, Naliboff BD, Craig ADB. Neuroimaging of the brain-gut axis: From basic understanding to treatment of functional G1 disorders. Gastroenterology. 2006;131(6):1925-42.

71. Derbyshire SW. A systematic review of neuroimaging data during visceral stimulation. Am J Gastroenterol. 2003;98(1):12-20.

72. Mayer EA, Aziz Q, Coen S, Kern M, Labus JS, Lane R, et al. Brain imaging approaches to the study of functional GI disorders: A Rome Working Team Report. Neurogastroent Motil. 2009;21(6):579-96.

73. Gregory LJ, Yaguez L, Williams SC, Altmann C, Coen SJ, Ng V, et al. Cognitive modulation of the cerebral processing of human oesophageal sensation using functional magnetic resonance imaging. Gut. 2003;52(12):1671-7.

74. Van Oudenhove L, McKie S, Lassman D, Uddin B, Paine P, Coen S, et al. Fatty acid-induced gut-brain signaling attenuates neural and behavioral effects of sad emotion in humans. J Clin Invest. 2011;121(8):3094-9.

75. Yaguez L, Coen S, Gregory LJ, Amaro E, Jr., Altman C, Brammer MJ, et al. Brain response to visceral aversive conditioning: a functional magnetic resonance imaging study. Gastroenterology. 2005;128(7):1819-29.

76. Hall GB, Kamath MV, Collins S, Ganguli S, Spaziani R, Miranda KL, et al. Heightened central affective response to visceral sensations of pain and discomfort in IBS. Neurogastroenterol Motil. 2010;22(3):276-e80.

77. Hojo M, Takahashi T, Nagahara A, Sasaki H, Oguro M, Asaoka D, et al. Analysis of brain activity during visceral stimulation. J Gastroenterol Hepatol. 2012;27 Suppl 3:49-52.

78. Zempleni MZ, Michels L, Mehnert U, Schurch B, Kollias S. Cortical substrate of bladder control in SCI and the effect of peripheral pudendal stimulation. Neuroimage. 2010;49(4):2983-94.

79. Cardinal RN, Parkinson JA, Hall J, Everitt BJ. Emotion and motivation: the role of the amygdala, ventral striatum, and prefrontal cortex. Neurosci Biobehav Rev. 2002;26(3):321-52.

80. Griffiths DJ. Cerebral control of bladder function. Curr Urol Rep. 2004;5(5):348-52.

81. Labus JS, Naliboff BN, Fallon J, Berman SM, Suyenobu B, Bueller JA, et al. Sex differences in brain activity during aversive visceral stimulation and its expectation in patients with chronic abdominal pain: a network analysis. Neuroimage. 2008;41(3):1032-43.

82. Naliboff BD, Berman S, Chang L, Derbyshire SW, Suyenobu B, Vogt BA, et al. Sex-related differences in IBS patients: central processing of visceral stimuli. Gastroenterology. 2003;124(7):1738-47.

83. Seseke S, Baudewig J, Kallenberg K, Ringert RH, Seseke F, Dechent P. Gender differences in voluntary micturition control: an fMRI study. Neuroimage. 2008;43(2):183-91.

84. Jackson S, Donovan J, Brookes S, Eckford S, Swithinbank L, Abrams P. The Bristol Female Lower Urinary Tract Symptoms questionnaire: development and psychometric testing. Br J Urol. 1996;77(6):805-12.

85. Abrams P, Feneley R, Torrens M. Urodynamics. London: Springer. 2006.

86. Abrams P, Cardozo L, Fall M, Griffiths D, Rosier P, Ulmsten U, et al. The standardisation of terminology of lower urinary tract function: report from the Standardisation Sub-committee of the International Continence Society. Am J Obstet Gynecol. 2002;187(1):116-26.

87. Chancellor MB, Lavelle J, Ozawa H, Jung SY, Watanabe T, Kumon H. Ice-water test in the urodynamic evaluation of spinal cord injured patients. Tech Urol. 1998;4(2):87-91.

88. Geirsson G, Fall M, Lindstrom S. The ice-water test--a simple and valuable supplement to routine cystometry. Br J Urol. 1993;71(6):681-5.

89. Bors E, Parker R. Observations on some modalities of bladder sensation. J Urol. 1956;76:566–75.

90. Nathan PW. Thermal sensation in the bladder. J Neurol Neurosurg Psychiatry. 1952;15(3):150-1.

91. Tammela TL, Hellstrom PA, Kontturi MJ. Cold sensation and bladder instability in patients with outflow obstruction due to benign prostatic hyperplasia. Br J Urol. 1992;70(4):404-7.

92. Mukerji G, Waters J, Chessell IP, Bountra C, Agarwal SK, Anand P. Pain during ice water test distinguishes clinical bladder hypersensitivity from overactivity disorders. BMC Urol. 2006;6:31.

93. Burnstock G. Physiology and pathophysiology of purinergic neurotransmission. Physiol Rev. 2007;87(2):659-797.

94. Powell-Boone T, Ness TJ, Cannon R, Lloyd LK, Weigent DA, Fillingim RB. Menstrual cycle affects bladder pain sensation in subjects with interstitial cystitis. J Urol. 2005;174(5):1832-6.

95. Jarrahi B, Wanek J. Design of an fMRI-compatible optical touch stripe based on frustrated total internal reflection. Conf Proc IEEE Eng Med Biol Soc. 2014;2014:4952-5.

96. Jarrahi B, Wanek J, Mehnert U, Kollias S. An fMRI-compatible multi-configurable handheld response system using an intensity-modulated fiber-optic sensor. Conf Proc IEEE Eng Med Biol Soc. 2013;2013:6349-52.

97. Friston KJ, Ashburner J, Frith CD, Poline JP, Heather JD, Frackowiak RS. Spatial registration and normalization of images. Human Brain Mapp. 1995;3:165-89.

98. Sladky R, Friston KJ, Trostl J, Cunnington R, Moser E, Windischberger C. Slice-timing effects and their correction in functional MRI. Neuroimage. 2011;58(2):588-94.

99. Allen EA, Erhardt EB, Damaraju E, Gruner W, Segall JM, Silva RF, et al. A baseline for the multivariate comparison of resting-state networks. Front Syst Neurosci. 2011;5:2.

100. Zuo XN, Kelly C, Adelstein JS, Klein DF, Castellanos FX, Milham MP. Reliable intrinsic connectivity networks: test-retest evaluation using ICA and dual regression approach. Neuroimage. 2010;49(3):2163-77.

101. Thomas CG, Harshman RA, Menon RS. Noise reduction in BOLD-based fMRI using component analysis. Neuroimage. 2002;17(3):1521-37.

102. De Luca M, Beckmann CF, De Stefano N, Matthews PM, Smith SM. fMRI resting state networks define distinct modes of long-distance interactions in the human brain. Neuroimage. 2006;29(4):1359-67.

103. Koch W, Teipel S, Mueller S, Buerger K, Bokde AL, Hampel H, et al. Effects of aging on default mode network activity in resting state fMRI: does the method of analysis matter? Neuroimage. 2010;51(1):280-7.

104. Herbert BM, Muth ER, Pollatos O, Herbert C. Interoception across modalities: on the relationship between cardiac awareness and the sensitivity for gastric functions. PLoS One. 2012;7(5):e36646.

105. Pollatos O, Kirsch W, Schandry R. Brain structures involved in interoceptive awareness and cardioafferent signal processing: a dipole source localization study. Hum Brain Mapp. 2005;26(1):54-64.

106. Schandry R. Heart beat perception and emotional experience. Psychophysiology. 1981;18(4):483-8.

107. Wiens S, Mezzacappa ES, Katkin ES. Heartbeat detection and the experience of emotions. Cognition Emotion. 2000;14(3):417-27.

108. Arbabshirani MR, Havlicek M, Kiehl KA, Pearlson GD, Calhoun VD. Functional network connectivity during rest and task conditions: a comparative study. Hum Brain Mapp. 2013;34(11):2959-71.

109. Li YO, Adali T, Calhoun VD. Estimating the number of independent components for functional magnetic resonance Imaging data. Human Brain Mapping. 2007;28(11):1251-66.

110. Li YO, Adah T, Calhoun VD. Sample dependence correction for order selection in fMRI analysis. I S Biomed Imaging. 2006:1072-+.

111. Bell AJ, Sejnowski TJ. An information-maximization approach to blind separation and blind deconvolution. Neural Comput. 1995;7(6):1129-59.

112. Himberg J, Hyvarinen A, Esposito F. Validating the independent components of neuroimaging time series via clustering and visualization. Neuroimage. 2004;22(3):1214-22.

113. Erhardt EB, Rachakonda S, Bedrick EJ, Allen EA, Adali T, Calhoun VD. Comparison of multi-subject ICA methods for analysis of fMRI data. Hum Brain Mapp. 2011;32(12):2075-95.

114. Calhoun VD, Kiehl KA, Liddle PF, Pearlson GD. Aberrant localization of synchronous hemodynamic activity in auditory cortex reliably characterizes schizophrenia. Biol Psychiatry. 2004;55(8):842-9.

115. Calhoun VD, Pekar JJ, Pearlson GD. Alcohol intoxication effects on simulated driving: exploring alcohol-dose effects on brain activation using functional MRI. Neuropsychopharmacology. 2004;29(11):2097-17.

116. Ma S, Correa NM, Li XL, Eichele T, Calhoun VD, Adali T. Automatic Identification of Functional Clusters in fMRI Data Using Spatial Dependence. Ieee T Bio-Med Eng. 2011;58(12):3406-17.

117. Meda SA, Stevens MC, Folley BS, Calhoun VD, Pearlson GD. Evidence for Anomalous Network Connectivity during Working Memory Encoding in Schizophrenia: An ICA Based Analysis. Plos One. 2009;4(11).

118. Zhang S, Li CS. Functional networks for cognitive control in a stop signal task: independent component analysis. Hum Brain Mapp. 2012;33(1):89-104.

119. Cordes D, Haughton VM, Arfanakis K, Wendt GJ, Turski PA, Moritz CH, et al. Mapping functionally related regions of brain with functional connectivity MR imaging. AJNR Am J Neuroradiol. 2000;21(9):1636-44.

120. Beckmann CF, Mackay CE, Filippini N, Smith SM. Group comparison of resting-state FMRI data using multi-subject ICA and dual regression. Neuroimage. 2009;47:148.

121. D'Argembeau A, Collette F, Van der Linden M, Laureys S, Del Fiore G, Degueldre C, et al. Self-referential reflective activity and its relationship with rest: a PET study. Neuroimage. 2005;25(2):616-24.

122. Damoiseaux JS, Rombouts SA, Barkhof F, Scheltens P, Stam CJ, Smith SM, et al. Consistent resting-state networks across healthy subjects. Proc Natl Acad Sci U S A. 2006;103(37):13848-53.

123. Kiviniemi V, Starck T, Remes J, Long X, Nikkinen J, Haapea M, et al. Functional segmentation of the brain cortex using high model order group PICA. Hum Brain Mapp. 2009;30(12):3865-86.

124. Laird AR, Fox PM, Eickhoff SB, Turner JA, Ray KL, McKay DR, et al. Behavioral interpretations of intrinsic connectivity networks. J Cogn Neurosci. 2011;23(12):4022-37.

125. Mantini D, Perrucci MG, Del Gratta C, Romani GL, Corbetta M. Electrophysiological signatures of resting state networks in the human brain. P Natl Acad Sci USA. 2007;104(32):13170-5.

126. Mantini D, Corbetta M, Romani GL, Orban GA, Vanduffel W. Evolutionarily Novel Functional Networks in the Human Brain? Journal of Neuroscience. 2013;33(8):3259-75.

127. Seeley WW, Menon V, Schatzberg AF, Keller J, Glover GH, Kenna H, et al. Dissociable intrinsic connectivity networks for salience processing and executive control. J Neurosci. 2007;27(9):2349-56.

128. Beckmann CF, DeLuca M, Devlin JT, Smith SM. Investigations into resting-state connectivity using independent component analysis. Philos Trans R Soc Lond B Biol Sci. 2005;360(1457):1001-13.

129. Smith SM, Jenkinson M, Woolrich MW, Beckmann CF, Behrens TE, Johansen-Berg H, et al. Advances in functional and structural MR image analysis and implementation as FSL. Neuroimage. 2004;23 Suppl 1:S208-19.

130. Woolrich MW, Jbabdi S, Patenaude B, Chappell M, Makni S, Behrens T, et al. Bayesian analysis of neuroimaging data in FSL. Neuroimage. 2009;45(1):S173-S86.

131. Fukunaga M, Horovitz SG, van Gelderen P, de Zwart JA, Jansma JM, Ikonomidou VN, et al. Large-amplitude, spatially correlated fluctuations in BOLD fMRI signals during extended rest and early sleep stages. Magn Reson Imaging. 2006;24(8):979-92.

132. Vincent JL, Patel GH, Fox MD, Snyder AZ, Baker JT, Van Essen DC, et al. Intrinsic functional architecture in the anaesthetized monkey brain. Nature. 2007;447(7140):83-6.

133. Eickhoff SB, Stephan KE, Mohlberg H, Grefkes C, Fink GR, Amunts K, et al. A new SPM toolbox for combining probabilistic cytoarchitectonic maps and functional imaging data. Neuroimage. 2005;25(4):1325-35.

134. Friston KJ, Holmes AP, Worsley KJ, Poline JP, Frith CD, Frackowiak RS. Statistical parametric maps in functional imaging: A general linear approach. Human Brain Mapping. 1994;2:189-210.

135. Handwerker DA, Ollinger JM, D'Esposito M. Variation of BOLD hemodynamic responses across subjects and brain regions and their effects on statistical analyses. Neuroimage. 2004;21(4):1639-51.

136. Genovese CR, Lazar NA, Nichols T. Thresholding of statistical maps in functional neuroimaging using the false discovery rate. Neuroimage. 2002;15(4):870-8.

137. Bressler SL, Menon V. Large-scale brain networks in cognition: emerging methods and principles. Trends Cogn Sci. 2010;14(6):277-90.

138. Greicius MD, Menon V. Default-mode activity during a passive sensory task: uncoupled from deactivation but impacting activation. J Cogn Neurosci. 2004;16(9):1484-92.

139. Raichle ME, MacLeod AM, Snyder AZ, Powers WJ, Gusnard DA, Shulman GL. A default mode of brain function. Proc Natl Acad Sci U S A. 2001;98(2):676-82.

140. Shulman GL, Fiez JA, Corbetta M, Buckner RL, Miezin FM, Raichle ME, et al. Common Blood Flow Changes across Visual Tasks: II. Decreases in Cerebral Cortex. J Cogn Neurosci. 1997;9(5):648-63.

141. Robinson S, Basso G, Soldati N, Sailer U, Jovicich J, Bruzzone L, et al. A resting state network in the motor control circuit of the basal ganglia. BMC Neurosci. 2009;10:137.

142. Menon V. Large-scale brain networks and psychopathology: a unifying triple network model. Trends Cogn Sci. 2011;15(10):483-506.

143. Menon V, Uddin LQ. Saliency, switching, attention and control: a network model of insula function. Brain Structure & Function. 2010;214(5-6):655-67.

144. Mutschler I, Wieckhorst B, Kowalevski S, Derix J, Wentlandt J, Schulze-Bonhage A, et al. Functional organization of the human anterior insular cortex. Neurosci Lett. 2009;457(2):66-70.

145. Seth AK, Suzuki K, Critchley HD. An interoceptive predictive coding model of conscious presence. Front Psychol. 2011;2:395.

146. Craig AD. How do you feel--now? The anterior insula and human awareness. Nat Rev Neurosci. 2009;10(1):59-70.

147. Critchley HD, Wiens S, Rotshtein P, Ohman A, Dolan RJ. Neural systems supporting interoceptive awareness. Nat Neurosci. 2004;7(2):189-95.

148. Harrison NA, Gray MA, Gianaros PJ, Critchley HD. The embodiment of emotional feelings in the brain. J Neurosci. 2010;30(38):12878-84.

149. Paulus MP, Stein MB. An insular view of anxiety. Biol Psychiatry. 2006;60(4):383-7.

150. Cauda F, Costa T, Torta DM, Sacco K, D'Agata F, Duca S, et al. Meta-analytic clustering of the insular cortex: characterizing the meta-analytic connectivity of the insula when involved in active tasks. Neuroimage. 2012;62(1):343-55.

151. Torta DM, Costa T, Duca S, Fox PT, Cauda F. Parcellation of the cingulate cortex at rest and during tasks: a meta-analytic clustering and experimental study. Front Hum Neurosci. 2013;7:275.

152. Herbert BM, Pollatos O. The body in the mind: on the relationship between interoception and embodiment. Top Cogn Sci. 2012;4(4):692-704.

153. Bechara A, Naqvi N. Listening to your heart: interoceptive awareness as a gateway to feeling. Nat Neurosci. 2004;7(2):102-3.

154. Botvinick MM, Cohen JD, Carter CS. Conflict monitoring and anterior cingulate cortex: an update. Trends Cogn Sci. 2004;8(12):539-46.

155. Carter CS, Botvinick MM, Cohen JD. The contribution of the anterior cingulate cortex to executive processes in cognition. Rev Neurosci. 1999;10(1):49-57.

156. Devinsky O, Morrell MJ, Vogt BA. Contributions of anterior cingulate cortex to behaviour. Brain. 1995;118 (Pt 1):279-306.

157. Asplund CL, Todd JJ, Snyder AP, Marois R. A central role for the lateral prefrontal cortex in goal-directed and stimulus-driven attention. Nat Neurosci. 2010;13(4):507-12.

158. Corbetta M, Patel G, Shulman GL. The reorienting system of the human brain: from environment to theory of mind. Neuron. 2008;58(3):306-24.

159. Fox MD, Corbetta M, Snyder AZ, Vincent JL, Raichle ME. Spontaneous neuronal activity distinguishes human dorsal and ventral attention systems. Proc Natl Acad Sci U S A. 2006;103(26):10046-51.

160. Downar J, Crawley AP, Mikulis DJ, Davis KD. A multimodal cortical network for the detection of changes in the sensory environment. Nat Neurosci. 2000;3(3):277-83.

161. Downar J, Crawley AP, Mikulis DJ, Davis KD. A cortical network sensitive to stimulus salience in a neutral behavioral context across multiple sensory modalities. J Neurophysiol. 2002;87(1):615-20.

162. DiQuattro NE, Geng JJ. Contextual knowledge configures attentional control networks. J Neurosci. 2011;31(49):18026-35.

163. Dias R, Robbins TW, Roberts AC. Dissociation in prefrontal cortex of affective and attentional shifts. Nature. 1996;380(6569):69-72.

164. Frith C, Dolan R. The role of the prefrontal cortex in higher cognitive functions. Brain Res Cogn Brain Res. 1996;5(1-2):175-81.

165. Aziz Q, Thompson DG, Ng VW, Hamdy S, Sarkar S, Brammer MJ, et al. Cortical processing of human somatic and visceral sensation. J Neurosci. 2000;20(7):2657-63.

166. Peyron R, Laurent B, Garcia-Larrea L. Functional imaging of brain responses to pain. A review and meta-analysis (2000). Neurophysiol Clin. 2000;30(5):263-88.

167. Duncan J, Owen AM. Common regions of the human frontal lobe recruited by diverse cognitive demands. Trends Neurosci. 2000;23(10):475-83.

168. Gilbert SJ, Simons JS, Frith CD, Burgess PW. Performance-related activity in medial rostral prefrontal cortex (area 10) during low-demand tasks. J Exp Psychol Hum Percept Perform. 2006;32(1):45-58.

169. Spreng RN, Mar RA, Kim AS. The common neural basis of autobiographical memory, prospection, navigation, theory of mind, and the default mode: a quantitative meta-analysis. J Cogn Neurosci. 2009;21(3):489-510.

170. Uddin LQ, Kelly AM, Biswal BB, Castellanos FX, Milham MP. Functional connectivity of default mode network components: correlation, anticorrelation, and causality. Hum Brain Mapp. 2009;30(2):625-37.

171. Blok BF, Holstege G. Direct projections from the periaqueductal gray to the pontine micturition center (M-region). An anterograde and retrograde tracing study in the cat. Neurosci Lett. 1994;166(1):93-6.

172. Cabanac M. Physiological role of pleasure. Science. 1971;173(4002):1103-7.

173. Bechara A, Damasio H, Damasio AR. Emotion, decision making and the orbitofrontal cortex. Cereb Cortex. 2000;10(3):295-307.

174. Damasio AR. The somatic marker hypothesis and the possible functions of the prefrontal cortex. Philos Trans R Soc Lond B Biol Sci. 1996;351(1346):1413-20.

175. Griffiths DJ, Fowler CJ. The micturition switch and its forebrain influences. Acta Physiol (Oxf). 2013;207(1):93-109.

176. Andrew J, Nathan PW. Lesions on the Anterior Frontal Lobes and Disturbances of Micturition and Defaecation. Brain. 1964;87:233-62.

177. Mauricewilliams RS. Micturition Symptoms in Frontal Tumors. J Neurol Neurosur Ps. 1974;37(4):431-6.

178. Griffiths DJ, McCracken PN, Harrison GM, Gormley EA, Moore K, Hooper R, et al. Cerebral aetiology of urinary urge incontinence in elderly people. Age Ageing. 1994;23(3):246-50.

179. Sakakibara R, Hattori T, Yasuda K, Yamanishi T. Micturitional disturbance after acute hemispheric stroke: analysis of the lesion site by CT and MRI. J Neurol Sci. 1996;137(1):47-56.

180. de Groat WC, Griffiths D, Yoshimura N. Neural control of the lower urinary tract. Compr Physiol. 2015;5(1):327-96.

181. Northoff G, Heinzel A, de Greck M, Bermpohl F, Dobrowolny H, Panksepp J. Self-referential processing in our brain--a meta-analysis of imaging studies on the self. Neuroimage. 2006;31(1):440-57.

182. Kringelbach ML, Rolls ET. The functional neuroanatomy of the human orbitofrontal cortex: evidence from neuroimaging and neuropsychology. Prog Neurobiol. 2004;72(5):341-72.

183. Baldo BA, Kelley AE. Discrete neurochemical coding of distinguishable motivational processes: insights from nucleus accumbens control of feeding. Psychopharmacology (Berl). 2007;191(3):439-59.

184. Wise RA. Dopamine, learning and motivation. Nature Reviews Neuroscience. 2004;5(6):483-94.

185. James W. The physical basis of emotion. Pyschol Rev. 1994;101:205-10.

186. Lange. The Emotions. ML: Williams & Wilkins. 1992.

187. Bechara A. The role of emotion in decision-making: evidence from neurological patients with orbitofrontal damage. Brain Cogn. 2004;55(1):30-40.

188. Gallese V, Keysers C, Rizzolatti G. A unifying view of the basis of social cognition. Trends Cogn Sci. 2004;8(9):396-403.

189. Amodio DM, Frith CD. Meeting of minds: the medial frontal cortex and social cognition. Nat Rev Neurosci. 2006;7(4):268-77.

190. Krhut J, Holy P, Tintera J, Zachoval R, Zvara P. Brain activity during bladder filling and pelvic floor muscle contractions: a study using functional magnetic resonance imaging and synchronous urodynamics. Int J Urol. 2014;21(2):169-74.

191. Dutta A, McKie S, Deakin JF. Resting state networks in major depressive disorder. Psychiatry Res. 2014;224(3):139-51.

192. Cetin MS, Christensen F, Abbott CC, Stephen JM, Mayer AR, Canive JM, et al. Thalamus and posterior temporal lobe show greater inter-network connectivity at rest and across sensory paradigms in schizophrenia. Neuroimage. 2014;97:117-26.

193. Beldzik E, Domagalik A, Daselaar S, Fafrowicz M, Froncisz W, Oginska H, et al. Contributive sources analysis: a measure of neural networks' contribution to brain activations. Neuroimage. 2013;76:304-12.

194. Xu J, Zhang S, Calhoun VD, Monterosso J, Li CS, Worhunsky PD, et al. Task-related concurrent but opposite modulations of overlapping functional networks as revealed by spatial ICA. Neuroimage. 2013;79:62-71.

195. de Groat WC, Steers W. Autonomic regulation of the urinary bladder and sexual organs. In: Loewy AD, Spyer KM, editor. Central Regulation of Autonomic Functions. New York: Oxford University Press. 1990:310–33.

196. Hamdy S, Enck P, Aziz Q, Uengoergil S, Hobson A, Thompson DG. Laterality effects of human pudendal nerve stimulation on corticoanal pathways: evidence for functional asymmetry. Gut. 1999;45(1):58-63.

197. Nishizawa O, Ebina K, Sugaya K, Noto H, Satoh K, Kohama T, et al. Effect of cerebellectomy on reflex micturition in the decerebrate dog as determined by urodynamic evaluation. Urol Int. 1989;44(3):152-6.

198. Kucyi A, Hodaie M, Davis KD. Lateralization in intrinsic functional connectivity of the temporoparietal junction with salience- and attention-related brain networks. J Neurophysiol. 2012;108(12):3382-92.

199. Björnsdotter M, Löken L, Olausson H, Vallbo A, Wessberg J. Somatotopic organization of gentle touch processing in the posterior insular cortex. J Neurosci. 2009;29(29):9314-9320.

200. Liu P, Qin W, Wang J, Zeng F, Zhou G, Wen H, von Deneen KM, Liang F, Gong Q, Tian J. Identifying neural patterns of functional dyspepsia using multivariate pattern analysis: A resting-state fMRI study. PloS One. 2013;8(7)e68205.

201. Ueki K. Disturbances of micturition observed in some patients with brain tumor. Neurol Medico-Chirurgica. 1960;2(1-2):25-33

SUPPORTING INFORMATION

Supporting Table 1: **Participant's data including age and the urodynamic data comprising the maximum cystometric capacity (MCC), and the prefilled UB volume for strong desire to void to occur.**

Subject	Age	MCC [mL]	Prefill volume [mL]
1	48	920	600
2	21	770	300
3	45	545	500
4	30	700	400
5	24	480	300
6	26	680	400
7	24	815	450
8	24	705	600
9	27	750	600
10	22	500	400
11	21	520	500
12	31	640	500
13	30	645	500
14	44	440	250
15	38	770	400
Average	30.33	658.67	446.67
SD	9.13	138.30	110.95

Supporting Figure 1

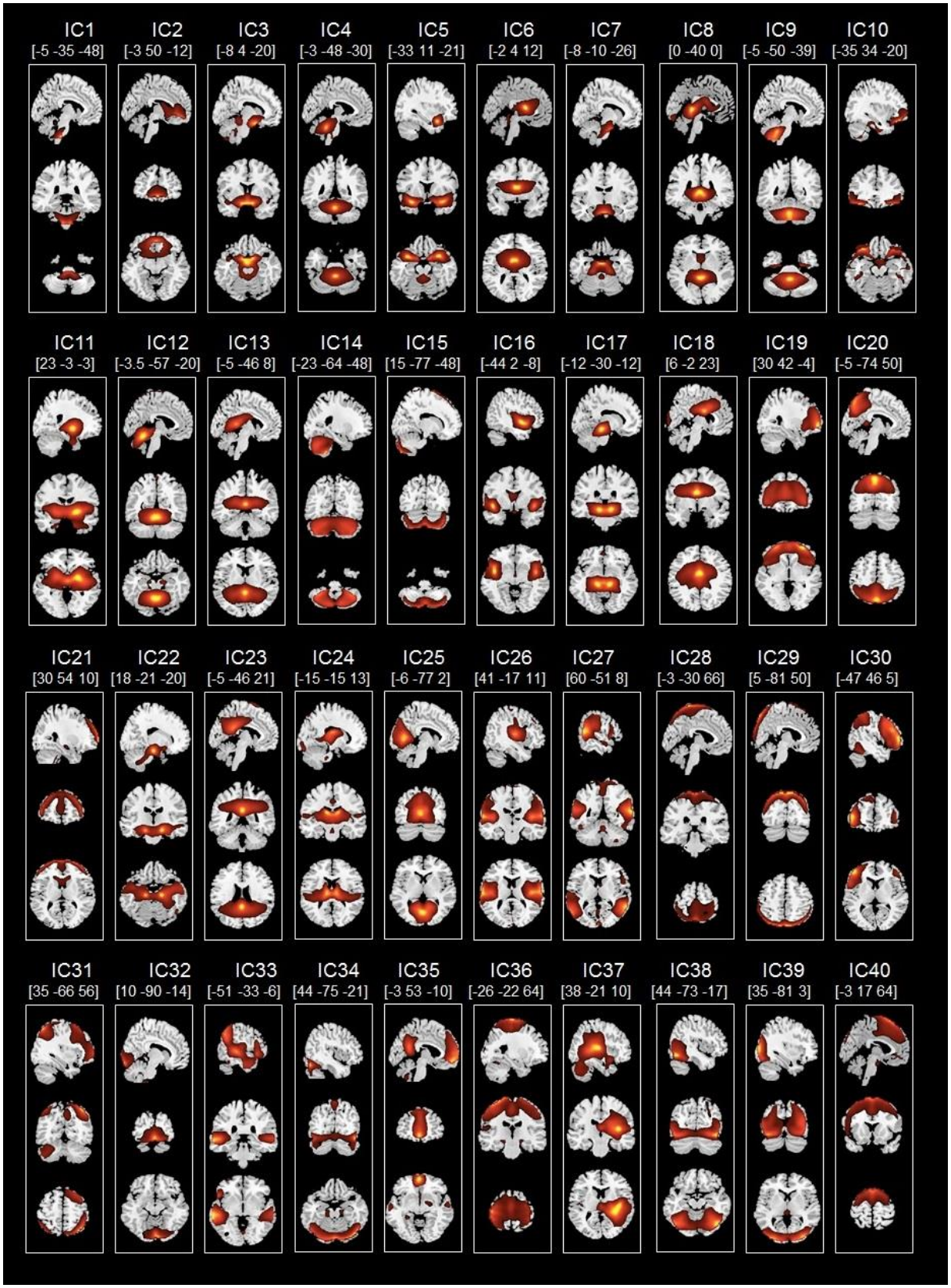

Supporting Figure 2

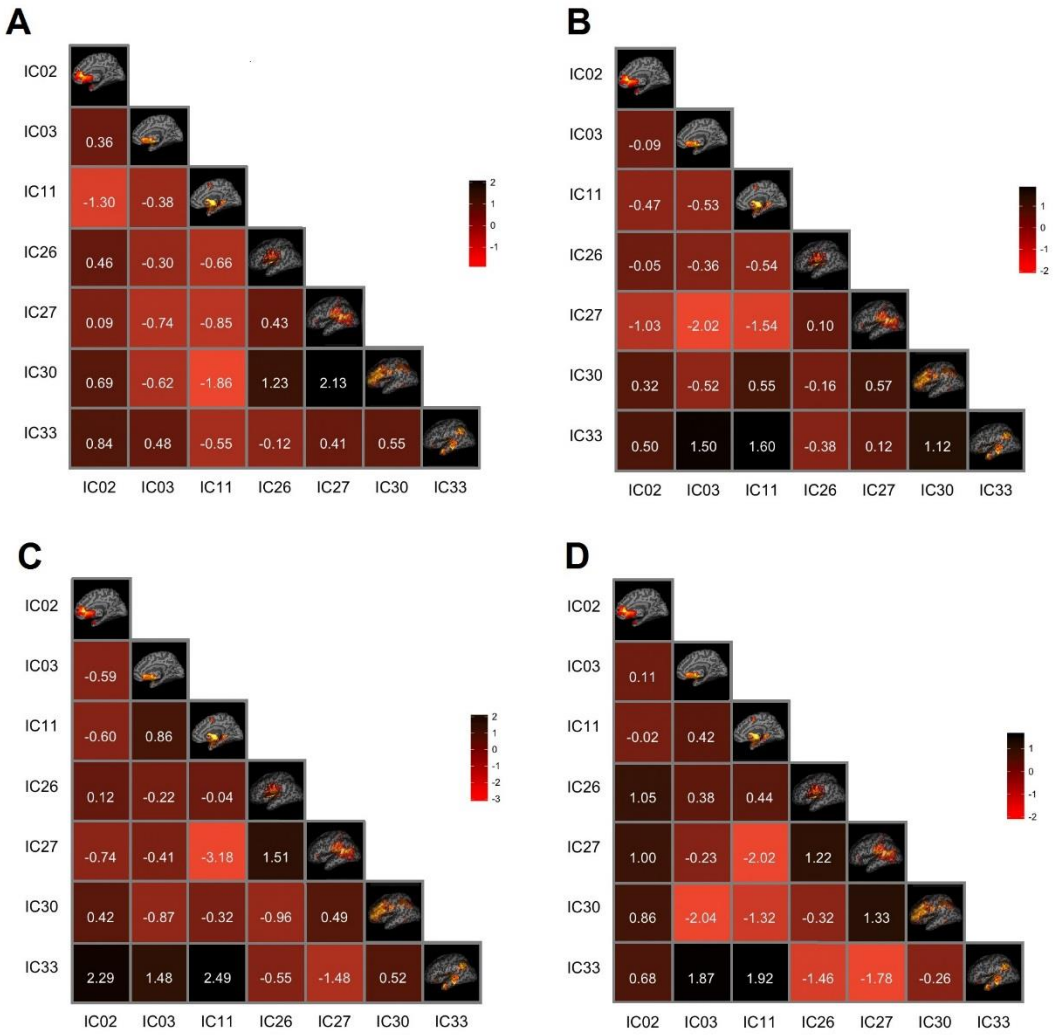

Supporting Figure 3

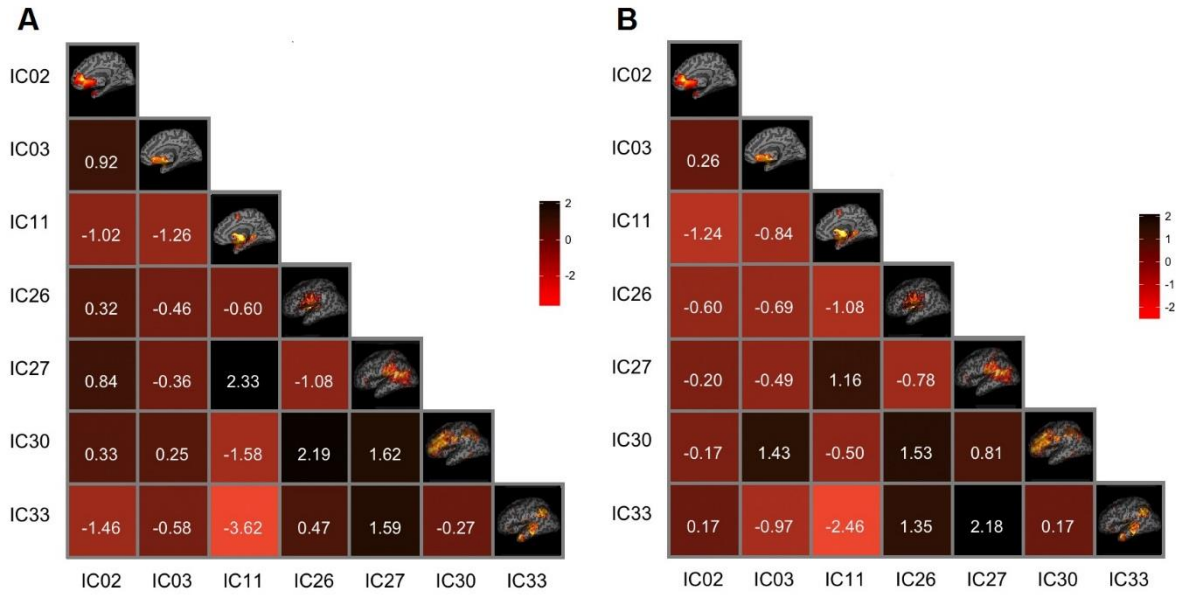

Supporting Figure 4